Gogny force with a finite-range density dependence

F. Chappert, N. Pillet,* M. Girod, and J.-F. Berger
CEA, DAM, DIF, F-91297 Arpajon, France

(Received 20 December 2013; revised manuscript received 12 December 2014; published 10 March 2015)

In the present work, we have investigated an extension of the effective nucleon-nucleon Gogny interaction in which the zero-range density-dependent term has been replaced with a finite-range term. The parameters have been adjusted on both nuclear-matter properties and a few observables of stable nuclei. The traditional and unified fitting procedure of the Gogny force used in Bruyères-le-Châtel ensures common basic properties between the extended analytical form of the Gogny interaction, called $D2$, and the original one. In particular, symmetric infinite nuclear-matter and neutron-matter properties as well as pairing correlations have been investigated. A few static properties obtained in finite nuclei using the Hartree-Fock-Bogoliubov approach and the $D2$ parametrization of the Gogny interaction are analyzed and compared to the results obtained with $D1$-type parametrizations and experiment when it is possible. The $D2$ parametrization makes it possible to reproduce nuclear structure properties with improved accuracy.

DOI: 10.1103/PhysRevC.91.034312 PACS number(s): 21.30.Fe, 21.10.−k, 21.60.Jz, 21.65.−f

I. INTRODUCTION

One of the great challenges of theoretical nuclear physics is to explain nuclear structure in terms of the nucleons and of their mutual interactions. Such a microscopic description of nuclei presents many advantages because it proposes a unified model from which we can deduce the properties of every nuclear system, even the most exotic nuclei and nuclear states unreachable experimentally. The difficulties of such a program are well known. First, the interaction between nucleons is not fundamental and it is necessary to determine *a priori* the analytical form to use in the many-body nuclear problem. Second, the solution of the quantum many-body problem is itself a difficult task.

The various studies realized in mean-field and beyond-mean-field theories to account for nuclear long-range correlations and using phenomenological interactions of Skyrme [1–14] and Gogny type [15–19] or those of the relativistic approach [20–22] demonstrate how powerful these methods are. They are applied to almost all nuclei, even the heaviest ones, and make it possible to interpret a considerable number of experimental data. One of the reasons for the good results provided by such an approach comes from the introduction of a density-dependent term in the parametrization of the effective interaction, which ensures the global properties of nuclei, in particular the saturation property. In the case of the Gogny [15] or Skyrme interactions, this dependence is proportional to ρ^{α}. In the Gogny interaction, $\alpha = 1/3$, whereas in the Skyrme interactions various values of α are used [23,24]. More recently, Hartree-Fock and Hartree-Fock-Bogoliubov calculations using a semirealistic nucleon-nucleon interaction corresponding to a modified version of the $M3Y$ interaction (introduction of a zero-range density-dependent term) have been achieved [25,26].

Such approaches raise the question of the interaction that has to be used in the effective Hamiltonian to describe the residual interaction, that is to say the nuclear long-range correlations (e.g., pairing correlations, collective oscillations of small and large amplitude, particle-vibration coupling). Focusing now on the Gogny interaction, the studies carried out with this interaction show that it is able to describe precisely at least the mean field of the nucleus, the pairing correlations, and the correlations induced by the collective oscillations of small [at the (quasiparticle) random phase approximation ((Q)RPA) level] and large [at the generator coordinate method (GCM) level] amplitudes [27–37].

The present work is a first step towards a new parametrization of the Gogny interaction in which all the components will have a finite range, including a complete refit of the interaction. Two main reasons can be invoked to justify this extension of the interaction. First, a finite-range interaction exhibits properties fundamentally different from a contact force at the mean-field approximation already. Especially, a zero-range force leads to a local mean field, while a finite-range force generates a nonlocal component—the exchange field—which significantly affects the single-particle state structure. The finite range of the effective nuclear force comes into play also in the intensity and the structure of the long-range correlations which affect the deformation properties of the nuclei [17]. The second reason is motivated by the use of the Gogny effective interaction in mean-field extensions, as (Q)RPA, second RPA [38–40], or configuration mixings of particle-hole type [41–43]. One way to render this point possible is to have a fully finite-range interaction for which the two-body residual matrix elements decrease naturally with the transferred momentum. We note also that there exists an attempt to go beyond the contact form within the Skyrme community [44,45], which reinforces the importance of the finite-range effects, long supported by the Gogny community.

The standard Gogny interaction has two zero-range terms: the density-dependent component and the spin-orbit component. The present work [46] is dedicated to the density-dependent term that presents a very different behavior in respect to the various nuclear long-range correlations. For the usual pairing correlations between like particles, some

*nathalie.pillet@cea.fr

theoretical arguments show that, at first order, the associated residual interaction is not—or very little—renormalized by the medium effects. We then expect that this part of the interaction is nearly independent of the density. This point is still under debate concerning the proton-neutron pairing. Alternatively, we know that the density-dependent component is essential for the description of RPA correlations when we use such interactions. The consistency between the HF and the RPA is essential to fulfill the sum rules, for which the rearrangement terms play a significant role, as shown in Refs. [27,28]. As can be expected, the density-dependent part can also play a very important role for more general correlations, such as particle-vibration coupling, for the renormalization of the mean-field one-particle states, as well as in odd-odd nuclei [47].

In the $D1$-type traditional parametrizations of the Gogny interaction [15–19,48,49], the action of the density-dependent component has been limited to the even-triplet channel of two-nucleon states such that only finite-range components of the force contribute to the pairing interaction. This limitation was necessary to apply the Hartree-Fock-Bogoliubov (HFB) method without any arbitrary truncation of the single-particle states space. However, such a limitation turns out to be too restrictive for the description of other correlations. In such cases, the density-dependent part should be also active in other two-nucleon states than the only even-triplet one. A finite-range density-dependent term has two consequences: the possibility to introduce a density dependence in all spin-isospin ST channels of the interaction and a nonpathological behavior of the residual matrix elements for high transferred momenta, as already mentioned.

As the spin-orbit term contributes weakly in the pairing field and its contribution in the particle-hole matrix elements is relatively small in the (Q)RPA and configuration mixing of particle-hole type approaches, for example, we have postponed to a future work the generalization of the spin-orbit component to a finite-range term including an isospin exchange component P_τ. We note that recently a version of the $D1$-type parametrizations containing a finite-range tensor term has been proposed, without a global refit of the interaction [50].

The article is organized as follows. In Sec. II, we discuss the new analytical form of the density-dependent term of the Gogny interaction. A few details concerning the fitting procedure of the Gogny interaction are recalled and the parameters of the new parametrization of the Gogny interaction, called $D2$ in the following, are provided. In Sec. III, the infinite nuclear-matter properties are presented for the $D2$ parametrizations. In particular, the equation of state, the incompressibility, the effective mass, the symmetry energy, the Landau parameters, and the pairing properties are discussed. A comparison with the $D1$-type parametrization (in particular, the $D1S$ one that is the most tested in various mean-field-based models) as well as empirical values is done. In Sec. IV, we first give computational details concerning the implementation of the finite-range and density-dependent terms in the axially deformed HFB code AMEDEE originally developed by Girod [51]. Then a few selected properties of finite nuclei are exposed. The pairing properties and the spin of odd isotopes in the Sn isotopic chain, the charge and neutron distributions in the Pb isotopic chain, the moments of inertia in rare-earth and actinide regions, and the fission barrier heights in actinides, calculated at the HFB approximation, are presented for the $D2$ parametrization. A comparison with the results obtained with the $D1$-type parametrizations is also done to make it credible. When it is possible, a comparison with experimental data is performed. Finally, conclusions and perspectives are given in Sec. V.

II. AN EXTENDED DENSITY-DEPENDENT GOGNY FORCE

A. Choice of the analytical form

In the present work, we propose to replace the analytical expression of the density-dependent term of the original Gogny interaction [17],

$$V_{\text{dens}}^{D1} = t_0\,(1 + x_0 P_\sigma)\,\delta\,(\vec{r}_1 - \vec{r}_2)\,\rho^\alpha\left(\frac{\vec{r}_1 + \vec{r}_2}{2}\right), \qquad (1)$$

with

$$V_{\text{dens}}^{D2} = (W_3 + B_3 P_\sigma - H_3 P_\tau - M_3 P_\sigma P_\tau) \times \frac{e^{-\frac{(\vec{r}_1 - \vec{r}_2)^2}{\mu_3^2}}}{(\mu_3\sqrt{\pi})^3}\,\frac{\rho^\alpha(\vec{r}_1) + \rho^\alpha(\vec{r}_2)}{2}, \qquad (2)$$

where the P_σ and P_τ operators are the spin and isospin exchange operators.

As the zero-range δ function $\delta(\vec{r}_1 - \vec{r}_2)$ suppresses any odd spatial component in the two-nucleon wave function, the expression (1) acts *a priori* in both the even-singlet ($S = 0,\ T = 1$) and even-triplet ($S = 1,\ T = 0$) channels. Furthermore, in the $D1$-type parametrizations, the parameter x_0 has been taken to be equal to 1 so that the contribution of the term (1) vanishes in the even-singlet channel ($S = 0, T = 1$). Such a choice was made by Gogny to avoid any divergences when the interaction is used to describe proton and neutron pairing correlations within the self-consistent HFB approach, assuming that the proton and the neutron pairings were close to the bare interaction.

The physical assumption underlying this choice was that the pairing correlations, which are a surface phenomenon, are not affected by medium effects at such densities. The finite range appearing in the expression (2) introduces odd and even spatial components. The new analytical form of the density-dependent term (2) allows all the spin-isospin exchanges and hence acts *a priori* in the four ST channels.

Two other finite-range density dependencies have also been investigated, namely with $\rho^\alpha(\frac{\vec{r}_1+\vec{r}_2}{2})$ and $\rho^{\frac{\alpha}{2}}(\vec{r}_1)\rho^{\frac{\alpha}{2}}(\vec{r}_2)$. All the three propositions are equivalent in the bulk of the nucleus but they can give different predictions when the interacting nucleons are closed to the surface. To choose between these three parametrizations, any physical criteria can hardly be invoked. Indeed, these expressions have been postulated and it is difficult to say which one simulates better the nucleon dynamics in the nucleus. So, we considered technical criteria to guide our choice, and it appeared that the parametrization (2) makes it easier to implement the fields in the HFB codes.

The new analytical expression of the Gogny interaction, called $D2$, is

$$V(|\vec{r}_1-\vec{r}_2|) = \sum_{i=1,2}(W_i + B_i P_\sigma - H_i P_\tau - M_i P_\sigma P_\tau) \times e^{-\frac{(\vec{r}_1-\vec{r}_2)^2}{\mu_i^2}} + (W_3 + B_3 P_\sigma - H_3 P_\tau - M_3 P_\sigma P_\tau) \times \frac{e^{-\frac{(\vec{r}_1-\vec{r}_2)^2}{\mu_3^2}}}{(\mu_3\sqrt{\pi})^3} \frac{\rho^\alpha(\vec{r}_1)+\rho^\alpha(\vec{r}_2)}{2} + i W_{LS} \overleftarrow{\nabla}_{12}\delta(\vec{r}_1-\vec{r}_2) \wedge \overrightarrow{\nabla}_{12}(\vec{\sigma}_1+\vec{\sigma}_2). \quad (3)$$

The third contribution in Eq. (3) corresponds to the spin-orbit term.

The $D2$ parametrization (3) of the Gogny interaction includes 17 parameters, namely, W_1, B_1, H_1, M_1, μ_1, W_2, B_2, H_2, M_2, μ_2, W_3, B_3, H_3, M_3, μ_3, α, and $W_{\rm LS}$. To adjust the values of these parameters, the original procedure proposed by Gogny [17] has been essentially kept. The additional parameters introduced in the new parametrization have been fitted by adding a few extensions to the original fitting procedure, as discussed in the following section.

B. Adjustment of the parameters

In the original fitting procedure of the Gogny interaction developed by Gogny [16], a set of equations that depends analytically on certain combinations of the parameters of the interaction is used to constrain them. These equations are chosen to govern the main nuclear properties so as to reproduce the most important experimental data.

The Hartree-Fock (HF) approximation is used and the single-particle wave functions are assumed to be the harmonic oscillator ones, an approximation known in the literature as the restricted HF approach. In this approach, four equations are related to the binding energies and the radii of two magic nuclei, namely, the ^{16}O and the ^{90}Zr. The constraint on the radii is directly related to the oscillator parameter $b = \sqrt{\hbar/M\omega}$, with ω the oscillator frequency and M the nucleon mass.

To govern the pairing properties of the interaction, two matrix elements are adjusted in the $1s$ and $2s$ states of the singlet-even channel ($S = 0$, $T = 1$). They provide two other equations. The values of these matrix elements are linked to the amplitude of the pairing gap in nuclei. The parameter x_0 is fixed equal to 1 to prevent a contribution of the density-dependent term to the pairing field.

To control the isospin properties of the interaction, the difference $\Delta\epsilon$ between the neutron and proton $2s_{1/2}$ single-particle energies in ^{48}Ca is adjusted to reproduce the empirical value of the symmetry energy. Recently, to complete this constraint [48], the fit of the neutron-matter equation of state has been added, leading to a new parametrization of the Gogny force, called $D1N$. To satisfy this new requirement, the value $\Delta\epsilon$ has been changed from the $D1S$ to the $D1N$ parametrization (from $\Delta\epsilon = -1.75$ MeV to $\Delta\epsilon = -2.60$ MeV). The drift appearing in the binding energies along isotopic chains when comparing theoretical results with the $D1S$ parametrization and experiment has been removed with the $D1N$ parametrization. The absence of this drift still manifests in the $D1M$ [49] and the $D2$ parametrizations of the Gogny interaction. These isospin properties give one additional equation.

TABLE I. Numerical values (in MeV) of the parameters W_i, B_i, H_i, and M_i of the central terms of the $D2$ Gogny interaction. The three ranges μ_i are expressed in fm.

i	μ_i	W_i	B_i	H_i	M_i
1	0.8	−1176.440	800.000	−927.366	1115.573
2	1.3	93.741	−162.161	122.414	−223.859
3	0.6	1800.000	600.000	400.000	−600.000

This system of seven equations does not constrain completely the whole set of parameters. For the central part of the interaction, the B_1 parameter and the ranges of the Gaussians, μ_1 and μ_2, are left free, such as the t_0 parameter of the density-dependent term. The exponent α of the density ρ is fixed to $1/3$. These parameters are chosen to provide an acceptable value of the incompressibility, the surface energy, and the binding energy in ^{208}Pb. Moreover, the intensity of the spin-orbit $W_{\rm LS}$ is chosen to reproduce the spin-orbit splitting in ^{16}O.

Finally, the main properties of the nuclear matter are controlled. In particular, as discussed in Sec. III, we check the saturation density, the total energy per particle, and its spin-isopsin contributions, the incompressibility, the effective mass, the symmetry energy and the Landau parameters.

With the finite-range and density-dependent term (2) of the $D2$ Gogny interaction, six parameters are involved: W_3, B_3, H_3, M_3, μ_3, and α. They replace the t_0, x_0, and α parameters of expression (1). As a first step, the parameters W_3, B_3, H_3, and M_3 have been adjusted in an indirect way in the present work, by selecting the combinations which reproduce correctly the neutron-matter equation of state and the behavior in the different ST channels in symmetric nuclear matter. The spin-orbit strength $W_{\rm LS}$ has been fixed to 130 MeV. Moreover, the power of the density in (2) has been kept equal to $1/3$. The values of the parameters W_i, B_i, H_i, and M_i of the central terms of the $D2$ parametrization are given in Table I.

III. INFINITE NUCLEAR MATTER WITH THE $D2$ GOGNY INTERACTION

A. Nuclear-matter properties

The main properties of the $D2$ Gogny interaction in symmetric nuclear matter—the saturation density ρ_0, the energy per particle E_0/A, the incompressibility K_∞, the effective mass m^*/m, and the symmetry energy a_τ—are presented in Table II and compared to the ones calculated with the $D1S$ parametrization. The *empirical* values are also indicated in the last column. The empirical saturation density ρ_0 is deduced from the charge distribution of heavy nuclei corrected from the effects of the Coulomb repulsion and the surface tension [52,53]. The energy per particle E_0/A and the symmetry energy a_τ appear explicitly in the semiempirical mass formula. Their empirical values are deduced from the adjustments of the mass formula [54–58] on the experimental

TABLE II. Nuclear-matter properties (see text) for the $D2$ and $D1S$ parametrizations of the Gogny interaction. The empirical values are also indicated in the last column.

	$D2$	$D1S$	Empirical value
$\rho_0(\mathrm{fm}^{-3})$	0.163	0.163	0.17 ($\pm$0.02)
E_0/A (MeV)	–16.00	–16.02	$-16(\pm1)$
K_∞ (MeV)	209	210	220 ($\pm$10)
m^*/m	0.74	0.70	0.70 ($\pm$0.05)
a_τ(MeV)	31.1	31.1	30 ($\pm$2)

binding energies. The incompressibility value K_∞ has been microscopically determined by Blaizot *et al.* [29] using different phenomenological effective interactions to correctly reproduce experimental data of heavy nuclei such as the energy of the breathing mode in ^{208}Pb. It was shown that the original range [210,220] MeV can be extended to [200,230] without spoiling the quality of the description of experimental data. This range of variation has still been used in the present fitting of the $D2$ interaction. Recent studies, done in the context of the Skyrme interactions, indicate that a larger value may be used [24]. Finally, the empirical value of the effective mass m^*/m has been deduced from the analysis of nucleon-nucleus scattering in the framework of the optical potential [59]. Concerning this point, a complementary study related to the calculation of the depth of the optical potential with the $D2$ interaction would be very meaningful.

From Table II, we see that the nuclear-matter properties of the $D2$ Gogny interaction are very similar to the well-known $D1S$ parametrization. Only the effective mass is slightly bigger. The differences between the $D2$ and the $D1N$ parametrizations arise from the incompressibility that is found bigger with $D1N$ (230 MeV vs 209 MeV) and the symmetry energy that is smaller by 1.4 MeV. All the values indicated in Table II are compatible with the empirical ones. A comparison between $D2$ and the $D1S$, $D1N$, and $D1M$ parametrizations displays only small differences regarding those global properties. This result was expected as a common fitting procedure has been used.

B. Equations of state

1. Symmetric matter

Originally, the Gogny interaction has been fitted using notably as a guide more fundamental calculations based on realistic two-body interactions and the Brueckner Hartree-Fock theory, in symmetric nuclear matter by ST channels [15–17]. In the present fit of the $D2$ interaction, we have followed the same approach but by replacing the old two-body G matrix with a more recent one [60,61]. It is only the general trend that is discussed in this context, as our interaction produces good saturation properties. In Fig. 1, we display the evolution of the potential energy according to the Fermi momentum k_F in the four ST channels. The results are presented for the $D1S$ (empty squares) and the $D2$ (empty circles) parametrizations. The predictions of Bethe-Brueckner-Goldstone (BBG) calculations based on the two-body AV14

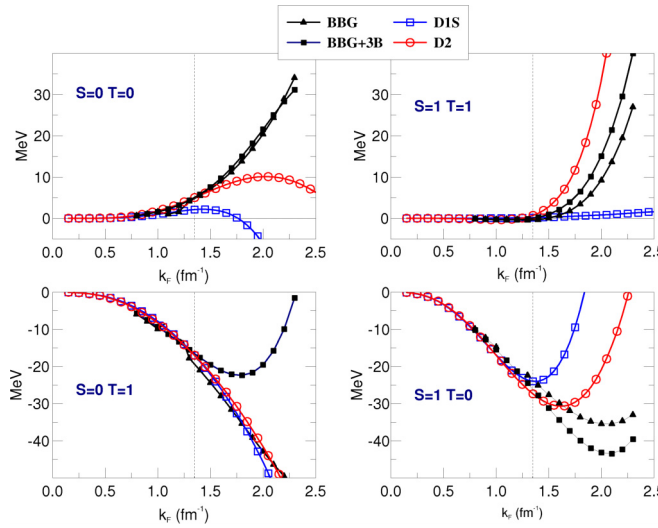

FIG. 1. (Color online) Potential energy in ST channels for the $D1S$ (empty squares) and $D2$ (empty circles) parametrizations of the Gogny interaction. The solid triangles and the solid squares correspond to Bethe-Brueckner-Goldstone calculations without and with 3-body interaction (BBG and BBG+3B respectively).

realistic interaction [62] (triangles) are shown [60,61]. For comparison, we have also indicated the predictions of BBG calculations including three-body (3B) force. In the range of interest for the fitting procedure of the Gogny interaction, going from the low-density regime up to densities around the saturation density, both BBG and BBG + 3B calculations predict similar results. Only BBG results are used for our comments. In each panel, the vertical dotted line indicates the saturation point at $k_F = 1.33$ fm^{-1}. We observe a general improvement of the behavior of the potential energy in the four ST channels with the $D2$ parametrization, in particular in odd ones.

In the odd-singlet channel ($S = 0, T = 0$), the microscopic BBG calculations predict a repulsive potential energy at any densities. The $D1S$ parametrization is in contradiction with these predictions by providing a strongly attractive potential energy beyond the Fermi momentum $k_F = 1.7$ fm^{-1}. The same pathology is present in the $D1N$ and $D1M$ parametrizations. With the $D2$ parametrization, this attractivity appears at very high momenta, beyond $k_F = 2.8$ fm^{-1}, or equivalently at $\rho = 9.3\rho_0$. At such densities, the quark dynamics play a role and the nucleons cannot be considered as the unique degrees of freedom of the theory. Our model is valid typically for densities up to a few times the saturation density. In this domain, the potential energy calculated with the $D2$ interaction is repulsive.

In the odd-triplet channel ($S = 1, T = 1$), we see that the $D1S$ parametrization gives a too-flat behavior in comparison with the BBG predictions, whereas the $D2$ parametrization displays a closer behavior, even though it is a little bit steeper. The attractivity of the $D2$ interaction (-0.3 MeV), developed around the saturation density, is in good agreement with the BBG predictions (-0.5 MeV).

In the even-singlet channel ($S = 0$, $T = 1$), the $D2$ interaction provides a potential energy curve very close to the ones associated with the $D1S$ parametrization. As we

see further when discussing the pairing properties in this channel, this property is explained by the very low intensity of the density dependence introduced by the $D2$ interaction in this channel. The two curves are also close to the BBG microscopic predictions, in low-density regime up to saturation density for which the pairing phenomenon might occur in finite nuclei.

In the even-triplet channel ($S = 1$, $T = 0$), the potential energy calculated with the $D1S$ parametrization follows the BBG trends up to the saturation density ρ_0. The $D2$ parametrization displays a behavior similar to the one of the BBG microscopic ones up to $k_F = 1.5$ fm^{-1}, corresponding to a density of $\rho = 1.4\rho_0$.

2. *Neutronic matter*

The control of the isospin dependence of the nuclear interaction is crucial, in particular in the study of the properties of nuclei along isotopic chains, moving from the stability line toward the drip lines. In this context, the investigation of the neutronic matter (simulating neutron-rich nuclei) is of primary interest [9,10,48].

The neutronic equation of state associated with the $D1S$ (empty squares) and $D2$ (empty circles) parametrizations is presented on the Fig. 2. The variational calculations of Friedman and Pandharipande (FP) (solid black curve) based on the AV14 realistic interaction are also indicated [63]. The $D2$ parametrization has been obtained by requiring that the FP neutron equation of state is reproduced within the error bars provided by their calculation. This constraint was absent in the original fitting procedure of the Gogny interaction, in particular in the fitting of the $D1S$ parametrization. For densities between $\rho_0/2$ and ρ_0, the $D2$ parametrization reproduces with less accuracy the FP curve but still within the error bars. However, beyond ρ_0, the $D2$ parametrization produces an equation of state capable of following the steep increase of the FP curve. Except at very low densities, the $D1S$ parametrization never displays a behavior compatible with the FP predictions, in particular the curvature appearing at $\sim\rho = \rho_0/2$.

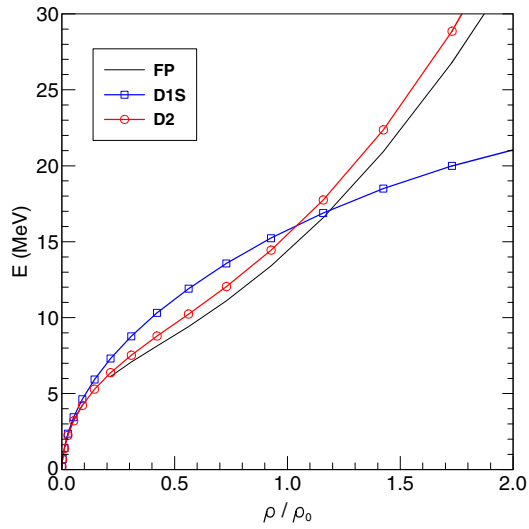

FIG. 2. (Color online) Equation of state of the neutronic matter for the $D1S$ (empty squares) and $D2$ (empty circles) parametrizations of the Gogny interaction. A comparison with the predictions of the variational Monte-Carlo approach (FP) by Friedman and Pandharipande (solid line) is done.

Systematic HFB calculations with the $D1S$ interaction have revealed a drift along isotopic chains when comparing experimental and theoretical binding energies. The merit of the $D1N$ parametrization [48], which fit in a very accurate way the neutronic equation of state, is to remove for the first time this drift produced by the Gogny interaction. The $D1M$ parametrization minimizes the difference to experiment ($\sim$798 keV) [49]. Because of the adding of the constraint on the neutronic equation of state, the drift is also absent with the $D2$ Gogny interaction [46]. However, the minimization of the difference to experiment was not one of the objectives of the present work and has been postponed for a future work.

C. Effective mass in asymmetric matter

In this part, we discuss the splitting of neutron and proton effective masses according to the asymmetry of the system that is defined by the parameter $\beta = (\rho_n - \rho_p)/\rho$, where ρ_n and ρ_p stand for the neutron and the proton densities. The microscopic theories based on the Brueckner-Hartree-Fock (BHF) approximation of the BBG approach [64,65] predict the neutron effective mass m^*_n/m to be greater than the proton effective mass m^*_p/m in neutron-rich matter. These theoretical predictions are confirmed by the phenomenological study of Li [66], who shows that the condition $m^*_n/m > m^*_p/m$ is necessary to obtain an energy dependence of the Lane potential in agreement with the experimental data on nucleon-nucleus scattering.

As seen from Table II, the effective mass m^*/m calculated in symmetric nuclear matter for the $D2$ parametrization (0.74) is a little higher than the value found with the $D1S$ parametrization (0.70). A small compression of proton and neutron spectra are expected with the $D2$ interaction in comparison with the $D1S$ one. The splitting of neutron (solid line) and proton (dashed line) effective masses in asymmetric matter is shown on Fig. 3 for the D1S (empty squares) and D2 (empty circles) parametrizations. The BHF predictions are also indicated (black). A global shift is obtained for proton and neutron effective masses between the two parametrizations.

For the maximal asymmetry $\beta = 1$ (neutron matter), the splitting obtained with the BHF-BBG calculations reaches $(m^*_n/m - m^*_p/m) = +0.16$. With the $D1S$ parametrization, the amplitude of the splitting is twice this value and keeps the same sign. For the new parametrization $D2$, the neutron effective mass is bigger than the proton one in agreement with the BHF-BBG predictions. The amplitude of the splitting obtained with $D2$ is close to the $D1S$ parametrization one with $(m^*_n/m - m^*_p/m) \simeq 0.30$ in neutron matter.

D. Landau parameters

Even though the determination of the numerical values of the parameters of the interaction is done essentially at the HF level, the Gogny interaction has been built from the beginning so that reasonable extensions beyond the HF approximation are meaningful. In particular, the RPA-type extensions to deal

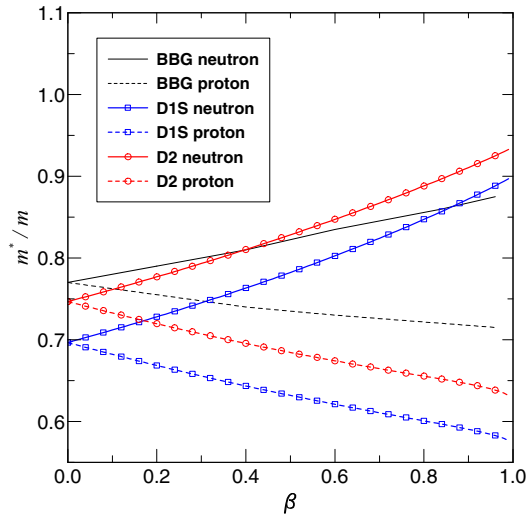

FIG. 3. (Color online) Neutron (solid line) and proton (dashed line) effective mass splitting as a function of the asymmetry β for the $D1S$ (empty squares) and $D2$ (empty circles) parametrizations of the Gogny interaction. The BBG microscopic predictions are indicated.

with collective excitations of small amplitude has been desired. Thus, the residual part of the Gogny interaction associated with this kind of nuclear long-range correlations has been controlled to satisfy this requirement. In that spirit, the calculations of Landau parameters with the different parametrizations of the Gogny interaction are crucial and used in the fitting procedure to select a parametrization. Indeed, at the limit of long wavelengths, Gogny and Padjen [28] have shown that, in infinite nuclear matter, the RPA equations reduce to Landau transport equations [67]. In that way, the Landau parameters can be determined from the nuclear effective interaction. Recently, a revival of the studies related to the Landau parameters of the effective interactions and, more generally, to the linear response theory can be noted [68–71].

To fix the notations, the residual interaction between Landau quasiparticles can be written as [72,73]

$$V(\vec{k},\vec{k}') = N^{-1}\{\mathcal{F}(\theta) + \mathcal{G}(\theta)\vec{\sigma}_1\cdot\vec{\sigma}_2 + \mathcal{F}'(\theta)\vec{\tau}_1\cdot\vec{\tau}_2 + \mathcal{G}'(\theta)\vec{\sigma}_1\cdot\vec{\sigma}_2\ \vec{\tau}_1\cdot\vec{\tau}_2\}, \quad (4)$$

where $\vec{k}$, $\vec{k}'$ are the wave vectors of the two interacting quasiparticles at the Fermi surface ($|\vec{k}| = |\vec{k}'| = k_F$), $N = 2m^*k_F/(\hbar^2\pi^2)$ is the density of states at the Fermi surface, and $\mathcal{F}(\theta)$, $\mathcal{G}(\theta)$, $\mathcal{F}'(\theta)$, and $\mathcal{G}'(\theta)$ are dimensionless functions of the angle θ between the vectors $\vec{k}$ and $\vec{k}'$.

The Landau parameters, noted $\mathcal{F}_l$, $\mathcal{G}_l$, $\mathcal{F}'_l$, and $\mathcal{G}'_l$ (l is the orbital angular momentum), are defined through an expansion in terms of the Legendre polynomial $P_l(\cos\theta)$ of $\mathcal{F}(\theta)$, $\mathcal{G}(\theta)$, $\mathcal{F}'(\theta)$, and $\mathcal{G}'(\theta)$,

$$\mathcal{F}(\theta) = \sum_{l=0}^{\infty}\mathcal{F}_l P_l(\cos\theta), \quad \mathcal{G}(\theta) = \sum_{l=0}^{\infty}\mathcal{G}_l P_l(\cos\theta),$$
$$\mathcal{F}'(\theta) = \sum_{l=0}^{\infty}\mathcal{F}'_l P_l(\cos\theta), \quad \mathcal{G}'(\theta) = \sum_{l=0}^{\infty}\mathcal{G}'_l P_l(\cos\theta). \quad (5)$$

In the following, we use for the Landau parameters the notation F_l^{ST} introduced by Gogny and Padjen [28], where S and T are the spin and the isospin of the particle-hole pair. The equivalence between the two notations is given by the relations

$$F_l^{00} \equiv \mathcal{F}_l, \quad F_l^{10} \equiv \mathcal{G}_l, \quad F_l^{01} \equiv \mathcal{F}'_l, \quad F_l^{11} \equiv \mathcal{G}'_l. \quad (6)$$

According to the derivation of Ref. [28], the Landau parameters F_l^{ST} are calculated from the second derivative of the energy.

For the $D1$-type parametrization, the explicit expressions of the Landau parameters are

$$F_0^{ST} = N\left\{\sum_{j=1}^{2} G_j(0)\left(A_j^{ST} + L_j^{(0)}B_j^{ST}\right) + t_0\rho_0^{\alpha}C^{ST}\right\},$$
$$F_{l\geqslant 1}^{ST} = N\left\{\sum_{j=1}^{2} L_j^{(l)}B_j^{ST}G_j(0)\right\}, \quad (7)$$

with ρ_0 the density of the system,

$$G_j(k) = (\mu_j\sqrt{\pi})^3 e^{-\frac{\mu_j^2}{2}k^2},$$
$$L_j^{(l)} = e^{-\frac{1}{2}\mu_j^2k_F^2}\left(l+\frac{1}{2}\right)\sum_{n=0}^{\infty}\frac{\left(\frac{\mu_j^2k_F^2}{4}\right)^{2n+l}}{n!(n+l+1/2)!}, \quad (8)$$

and

ST	A_j^{ST}	B_j^{ST}	C^{ST}
00	$W_j + \frac{B_j-H_j}{2} - \frac{M_j}{4}$	$M_j + \frac{H_j-B_j}{2} - \frac{W_j}{4}$	$\frac{3}{8}(\alpha+1)(\alpha+2)$
10	$\frac{B_j}{2} - \frac{M_j}{4}$	$\frac{H_j}{2} - \frac{W_j}{4}$	$\frac{x_0}{2} - \frac{1}{4}$
01	$-\frac{H_j}{2} - \frac{M_j}{4}$	$-\frac{B_j}{2} - \frac{W_j}{4}$	$-\frac{x_0}{2} - \frac{1}{4}$
11	$-\frac{M_j}{4}$	$-\frac{W_j}{4}$	$-\frac{1}{4}$

(9)

Because it can be checked easily, in the expression (7), the rearrangement terms and the second derivative of the energy according to the density act only for $l = 0$ and in the channel ($S = 0$, $T = 0$).

For the $D2$-type parametrization, the expressions of the Landau parameters are modified. Only the contributions related to the density-dependent term are different. We find

$$F_0^{ST} = N\left\{\sum_{j=1}^{2} G_j(0)\left(A_j^{ST} + L_j^{(0)} B_j^{ST}\right) + G_3^{'}(0)\left(A_3^{ST} + L_3^{(0)} B_3^{ST} + \delta_{S,0}\delta_{T,0} X_3^{00}\right)\right\},$$

$$F_{l\geqslant 1}^{ST} = N\sum_{j=1}^{2} L_j^{(l)} B_j^{ST} G_j(0) + L_3^{(l)} B_3^{ST} G_3^{'}(0), \tag{10}$$

with $G_3^{'}(0) = \rho_0^{\alpha} G_3(0)$ and $L_3^{(l)}$ is defined from the expression (8) for the range μ_3. The term X_3^{00} corresponds to the contribution of the rearrangement terms and the second derivative coming from the density-dependent term. It is equal to

$$X_3^{00} = 2\alpha A_3^{00} + 12\alpha(2\pi) B_3^{00}\int dr r^2 \frac{e^{-\frac{r^2}{\mu_3^2}}}{(\mu_3\sqrt{\pi})^3}\frac{j_1(k_F r)}{k_F r} j_0(k_F r) + \alpha(\alpha-1)\left\{\frac{1}{2}A_3^{00} + 9\pi^2 B_3^{00}\int dr r^2 \frac{e^{-\frac{r^2}{\mu_3^2}}}{(\mu_3\sqrt{\pi})^3}\left[\frac{j_1(k_F r)}{k_F r}\right]^2\right\}, \tag{11}$$

where the function $j_n(kr)$ are the spherical Bessel functions.

The values of the Landau parameters F_0^{ST} and F_1^{00} are presented in Table III for the $D1S$ and $D2$ parametrizations. The empirical values, determined by Speth, Zamick, and Ring [74–76] from the experimental properties of the collective states measured in ^{208}Pb (excitation energies, transition probabilities, ...), are indicated, as well as those deduced from Table II of Ref. [68].

The results obtained for the Landau parameter F_1^{00} with the $D1S$ and $D2$ parametrizations are found close but a little more negative with the $D1S$ parametrization because of its smaller effective mass. Indeed, the F_1^{00} Landau parameter and the effective mass are linked through the relation $m^*/m = 1 + F_1^{00}/3$ [77]. A comparison with both sets of empirical values indicates that the $D1S$ and the $D2$ parametrizations have compatible values for F_1^{00}, in particular with empirical value (2).

Concerning the F_0^{00} and F_0^{01} Landau parameters, the two parametrizations provide very similar values as the range of variation of the incompressibility K_∞ and the symmetry energy a_τ are narrow. Indeed, $K_\infty = 3\hbar^2 k_F^2(1 + F_0^{00})/m^*$ and $a_\tau = \hbar^2 k_F^2(1 + F_0^{01})/6m^*$ [77]. However, F_0^{00} always has the opposite sign, whatever the parametrization, if we consider the first set of empirical values, whereas it is strongly compatible with empirical value (2). To recover the empirical value (1), the incompressibility should be larger than 300 MeV, a requirement incompatible with the range determined by Blaizot *et al.* [29], whose deduced value is indicated in the last line of Table III.

TABLE III. Values of the Landau parameters, F_0^{00}, F_0^{10}, F_0^{01}, F_0^{11}, and F_1^{00}, calculated with the $D1S$ and $D2$ parametrizations of the Gogny interaction. Empirical values deduced from [74–76] and [68] are also indicated.

	F_0^{00}	F_0^{10}	F_0^{01}	F_0^{11}	F_1^{00}
$D1S$	−0.369	+0.466	+0.743	+0.631	−0.909
$D2$	−0.307	+0.198	+0.849	+0.962	−0.785
Empirical value (1) [74–76]	+0.1	+1.15	+0.7	+1.45	−0.6
Empirical value (2) [68]	−0.33		+0.8	+0.8	−0.9

For the F_0^{10} and F_0^{11} Landau parameters, they are not directly linked to physical quantities on which the parametrizations of the interaction have been adjusted. Hence, their values are very different from one parametrization to the other. The F_0^{11} parameter influences significantly the intensity and the energy of the Gamow-Teller resonance, especially in ^{208}Pb [68]. The $D2$ parametrization is expected to give a better description of this resonance.

In a general way, the calculated Landau parameters of the Gogny interactions are closer to the second set of empirical values.

The forward-scattering amplitude sum rule [28] is an interesting probe of the restoration, at least partial, of the antisymmetry of the scattering amplitude function Γ, also known as the total vertex function. The goal of this calculation is to verify to what extent phenomenological density-dependent effective interactions fulfill the elementary physical requirement that the forward-scattering amplitude of a particle-hole pair at the Fermi surface, at zero energy and zero momentum transfer for like particle and parallel spins, vanishes. This property is a direct consequence of the Pauli principle. Using an expansion with Legendre polynomials, we get the components of the total vertex function noted Γ_l^{ST}. The antisymmetry requirement leads to the general forward scattering amplitude sum rule $\sum_{l,ST}\Gamma_l^{ST} = 0$. More precisely, to ensure that the scattering amplitude of a particle-hole pair is antisymmetric in the exchange of two incoming or outgoing quasiparticles, two sum rules S_1 and S_2 [73] related to the Landau parameters can be built,

$$S_1 \equiv \sum_l \frac{F_l^{00}}{1 + F_l^{00}/(2l+1)} + \frac{F_l^{10}}{1 + F_l^{10}/(2l+1)} + \frac{F_l^{01}}{1 + F_l^{01}/(2l+1)} + \frac{F_l^{11}}{1 + F_l^{11}/(2l+1)},$$

$$S_2 \equiv \sum_l \frac{F_l^{00}}{1 + F_l^{00}/(2l+1)} - \frac{3F_l^{10}}{1 + F_l^{10}/(2l+1)} - \frac{3F_l^{01}}{1 + F_l^{01}/(2l+1)} + \frac{9F_l^{11}}{1 + F_l^{11}/(2l+1)}, \tag{12}$$

TABLE IV. S_1 and S_2 sum rules (see text) calculated with the $D1S$ and $D2$ parametrizations of the Gogny interaction.

	S_1	S_2
$D1S$	–0.162	–0.638
$D2$	0.014	–2.109

where each term of the summations corresponds to Γ_l^{ST}.

These S_1 and S_2 sum rules are related to the odd-triplet and odd-singlet channels in particle-particle coupling, respectively. To ensure that the scattering amplitude of two quasiparticles on the same state with momentum $\vec{k}$ is equal to zero for the odd partial waves, S_1 and S_2 have to be equal to zero. These sum rules do not concern the state with even parity as the scattering of two fermions on the same state with momentum $\vec{k}$ is not forbidden for the S partial wave. We note also that the antisymmetry requirement refers only to the total vertex function Γ_l^{ST} and not on the function F (F is not antisymmetric). Actually, there is no reason why it should be, because the F function is not a physically observable object. However, it is known that the rearrangement diagrams coming from the functional derivatives and included in the function F allow to restore, at least partially, the antisymmetry of the function Γ_l^{ST}.

The values of S_1 and S_2 are given in Table IV for the $D1S$ and $D2$ parametrizations. On the one hand, the first sum rule S_1 is well-verified by both parametrizations, and particularly by the $D2$ parametrization. On the other hand, the second sum rule S_2 is reproduced with much less accuracy for the different parametrizations. The $D1S$ parametrization provides the better result. The $D2$ parametrization introduces a much larger deviation, which will have to be improved.

Concerning the stability conditions established by Migdal [77], the Landau parameters have to satisfy the condition $F_l^{ST} > -(2l+1)$ in each ST channel and for any value of l. In Fig. 4, we display the evolution of the Landau parameters F_0^{ST} according to the density ρ normalized to the saturation density ρ_0 for the $D1S$ and $D2$ parametrizations. In that particular case, the stability condition gives $F_l^{ST} > -1$. At the saturation density, marked by arrows, this condition is satisfied for all the parametrizations in each ST channel. At low density, $\rho < 0.6\rho_0$, the stability condition is not verified in the $ST = 00$ channel for all the parametrizations. This isoscalar instability is dominated by fluctuations of the total density and can be interpreted as a liquid-gas phase transition (spinodal instability) [78–80]. For densities larger than the saturation density, some instabilities may develop for the $D1S$ parametrization. In the $ST = 01$ channel, the first instability appears at $\rho \equiv \rho_c^{D1S} = 3.4\rho_0$. In the $ST = 11$ channel, it appears at $\rho \equiv \rho_c^{D1S} = 2.0\rho_0$. On the contrary, the $D2$ parametrization predicts no instability at equivalent densities. The $D2$ parametrization which has a finite-range density-dependent term provides a nuclear matter more stable at high density than the standard $D1$-type parametrizations. In particular, the homogeneous, symmetric and nonmagnetic nuclear matter ($S = 0$) is stable at least at any density up to $\rho/\rho_0 \sim 6$ with the $D2$ parametrization [46].

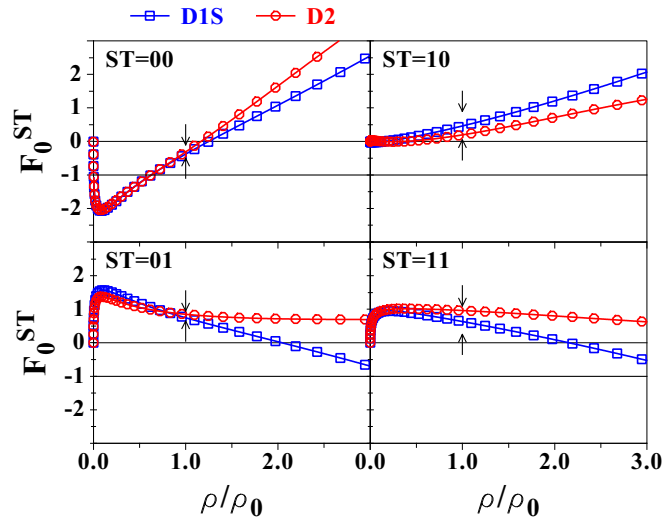

FIG. 4. (Color online) Landau parameters F_0^{ST} represented according the density, in each ST channels. The results have been obtained, in symmetric nuclear matter, with the $D1S$ (empty squares) and $D2$ (empty circles) parametrizations of the Gogny interaction.

E. Pairing properties in the $S = 0$, $T = 1$ channel

The pairing properties of the Gogny interaction in the $S = 0$, $T = 1$ channel is one of its main characteristics as this interaction has been designed to be able to treat both the mean and the pairing fields in a HFB approach. In this part, the $D1S$ parametrization is considered as the reference for the pairing properties in the $S = 0$, $T = 1$ channel. From our knowledge of the fitting of pairing correlations with the Gogny interaction, we have deduced two necessary conditions to obtain a realistic description of pairing in finite nuclei, in particular to avoid the appearance of pairing correlations in magic nuclei. If one of these two conditions is not fulfilled, then pairing correlations develop in magic nuclei.

The first necessary condition stems from the observation that the pairing energy in nuclei is very sensitive to the level of attractivity of the potential energy in the $S = 0, T = 1$ channel for densities ρ lower than $\rho_0/2$ ($k_F = 1.06$ fm^{-1}). Indeed, the relative contribution of parametrization to the potential energy in the subspace $S = 0$, $T = 1$ (see Fig. 1) makes it possible to presume the pairing properties of the parametrization. The potential energy in this subspace reflects the intensity of the pairing correlations, and thus it is deeply linked to the description of pairing correlations. Moreover, as the pairing manifests itself preferentially in the surface of nuclei where the density is lower, the low-density part of this subspace is the most determining one to adjust the pairing properties. We have studied the link between the level of attractivity of a Gogny parametrization in this $S = 0$, $T = 1$ subspace and the corresponding pairing correlations $E_{\rm app}$ obtained in ^{16}O using the HFB approach. The results are shown in Fig. 5. Clearly, we are able to fix a limit under which pairing correlations are predicted in the magic nuclei.

The second necessary condition concerns the spatial form of the pairing interaction that has to be similar to a molecular potential shape. In particular, a too-strong attraction (lower

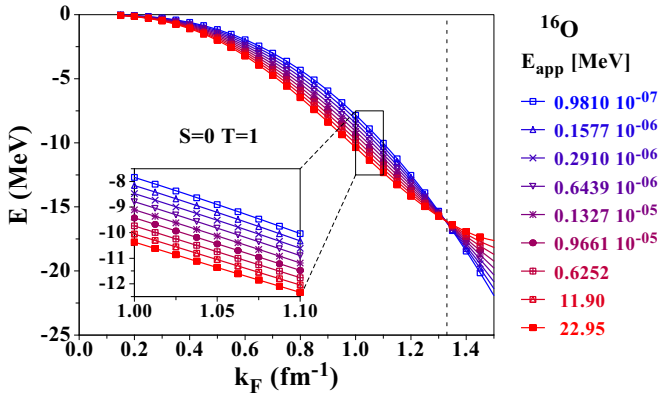

FIG. 5. (Color online) Contributions in the $S = 0, T = 1$ channel of various $D2$-type parametrizations of the Gogny force which differ only by the pairing attractivity.

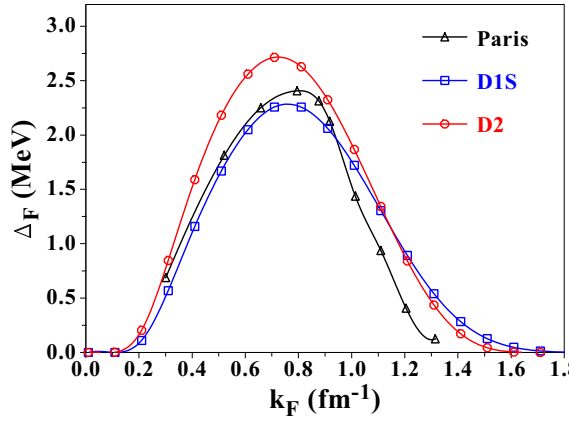

FIG. 7. (Color online) Pairing gap in $ST = 01$ channel, in symmetric nuclear matter, according to the Fermi momentum k_F. The results are shown for the $D1S$ (empty squares) and $D2$ (empty circles) parametrizations. The curve associated with the realistic Paris potential is also presented (solid line).

than -100 MeV) when the two nucleons are in contact creates a pathological pairing in finite nuclei. In Fig. 6, we display the spatial shape of the pairing interaction produced by the $D2$ parametrization for 100 densities ranging from 0 to ρ_0 with a step of $\Delta\rho = 0.01\rho_0$. The shape of the potential associated with the $D1S$ parametrization is also indicated (black circles). The crosses point out the minima. One sees that the $D2$ parametrization satisfies this second condition. At $r = 0$, the pairing interaction $V^{S=0,T=1}$ is always larger than ~ -100 MeV. One remarks that the potential is very sensitive to the density and consistent with the fact that contribution of the density dependence of the $D2$ parametrization has been chosen to be repulsive in the pairing channel. Finally, for the $D1S$ parametrization, the minimum is found at $r = 1.0$ fm. For the $D2$ parametrization, it ranges between 0.8 and 1.4 fm when ρ ranges from 0 to the saturation density ρ_0.

Another important piece of information related to the pairing interaction is given by the shape of the pairing gap Δ_F in nuclear matter as a function of the Fermi momentum k_F. In Fig. 7, one shows the evolution of the pairing gap Δ_F according to k_F in symmetric nuclear matter for the $D1S$ (empty squares) and the $D2$ (empty circles) parametrizations. The results of the realistic Paris interaction are also displayed (solid line) [81].

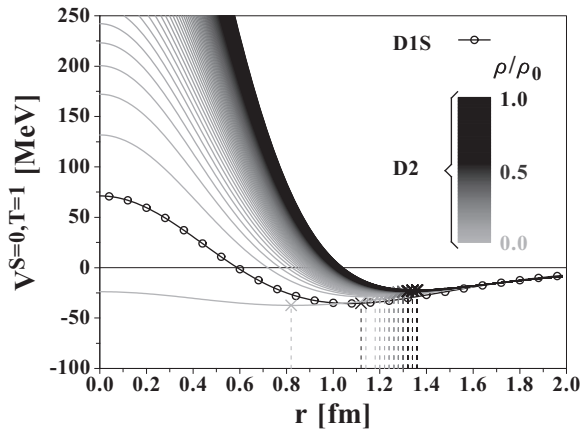

FIG. 6. Spatial shape of the pairing interaction for the $D1S$ (black open circles) and $D2$ parametrizations. On each curve, the crosses indicate the position of the minima.

If a parametrization of the Gogny interaction would reproduce, at all densities, the pairing gap of the realistic Paris interaction, it would not produce enough pairing in finite nuclei. To obtain enough pairing in nuclei, it is necessary that our parametrizations produce a gap greater than the one of the Paris interaction in a certain range of density. For the $D1S$ parametrization, this range concerns densities greater than $\rho_0/2$, the volume-pairing part. For the surface density, the $D1S$ parametrization is very similar to the bare interaction. The maximum of the curve is obtained at $k_F = 0.75$ fm^{-1} with a value around 2.3 MeV. The $D2$ parametrization has a relatively small repulsive contribution of the density-dependent term in the $ST = 01$ channel: $W_3 - B_3 - H_3 + M_3 = 200$ MeV fm$^{3(\alpha+1)}$. The shape of the gap is very similar to the one obtained with the $D1S$ parametrization. However, we note an amplitude that is a bit stronger ($\sim$2.7 MeV). To approach the curve of the gap obtained with the $D1S$ parametrization, it would have been sufficient to decrease the value of the combination of parameters $W_3 - B_3 - H_3 + M_3$ in the fitting procedure. The introduction of a slight repulsion for this combination of parameters has allowed to improve the behavior of the potential energy in all ST spin-isospin channels.

IV. A FEW FINITE NUCLEI PROPERTIES WITH THE $D2$ GOGNY INTERACTION

A. Computation details

The new analytical form $D2$ of the Gogny interaction proposed in this article has been implemented in the axially deformed HFB code with parity conservation, called AMEDEE [51], originally developed by Girod for the $D1$-type analytical form. In this code, the HFB equations are solved using an expansion on an axial harmonic oscillator (HO) basis with one center (see Appendix A). Moreover, only the pairing between like particles is considered. With the $D2$ interaction, the density-dependent term acts in both mean field and pairing

field. Because of its more general form, it brings contributions to the concerned neutron-neutron, proton-proton, and proton-neutron fields. The expressions of the fields are given in Appendix B. To program these expressions by optimizing the computation time to the maximum is a real challenge by itself. In the following, we describe the algorithm employed to implement the density-dependent term of the $D2$ Gogny interaction into the AMEDEE HFB code.

In the HFB method whose equations are solved in an iterative way, the convergence towards the self-consistent solutions is obtained when the coefficients $U_{\mu a}$ and $V_{\mu a}$ of the transformation between particles and quasiparticles operators (see Appendix B) no longer vary from one iteration to the other. To reach the self-consistent solution, up to 300 or 400 iterations are sometimes necessary. At each iteration, both the normal density ρ and the abnormal density κ as well as the fields Γ_{ac}, $\partial\Gamma_{ac}$, Δ_{ac}, and $\partial\Delta_{ac}$, expressed in the HO basis and defined in Appendix B, have to be calculated. As an example of computation time, we consider in the following the exchange part of the field Γ_{ac} in the case $m_a = m_c = m$ of Appendix B. As this term is the most difficult to calculate during one iteration, its computation time gives a good estimate of the speed of the code. In the following, we consider only the first term $\Gamma\,[1]^{q\Omega=m+s}_{m\nu_a,m\nu_c}(E)$ defined by [see Appendix B, Eq. (B38)]

$$\Gamma\,[1]^{q\Omega=m+s}_{m\nu_a,m\nu_c}(E) = \sum_{m'\geqslant 0\nu_b\nu_d} \langle m\nu_a m'\nu_b|G(r)F[\rho]|m'\nu_d m\nu_c\rangle \times R^{qs}_{m'\nu_d\nu_b}, \tag{13}$$

where $R^{qs}_{m'\nu_d\nu_b}$ contains the dependence in the density matrix ρ and is equal to

$$R^{qs}_{m'\nu_d\nu_b} = \sum_q \big[(M + H - (B + W)\delta_{qq'})\Theta(m' + s) \times \rho^{q'm'+s}_{m'\nu_d,m'\nu_b} + (M - B\delta_{qq'})\Theta(m' - s)\rho^{q'm'-s}_{m'\nu_d,m'\nu_b}\big]. \tag{14}$$

The m, m', and ν_i quantities represent the axial HO quantum numbers. Their meanings are explained in Appendix A. The index q is the projection of the isospin quantum number and s the projection of the intrinsic spin. Both take the values $\pm 1/2$.

Concerning the spatial part of the interaction, defined by the product $G(r)F[\rho]$, we have studied two cases, $G(r) = e^{-r^2/p^2}$ with $F[\rho] = 1$ and $G(r) = e^{-r^2/p^2}$ with $F[\rho] = [\rho^\alpha(\vec{r}_1) + \rho^\alpha(\vec{r}_2)]/2$. Here $\vec{r}$ represents the relative coordinates of the two-nucleon system. It is defined as $\vec{r} = \vec{r}_1 - \vec{r}_2$.

1. Case 1: $G(r) = e^{-r^2/p^2}$ and $F[\rho] = 1$

In this first considered case, the full expression of the interaction takes the form

$$\hat{v}_{12} = (W + B\hat{P}_\sigma - H\hat{P}_\tau - M\hat{P}_\sigma\hat{P}_\tau)e^{-r^2/p^2}. \tag{15}$$

According to Appendix B, the spatial part of the matrix element of the interaction (15), noted $\mathcal{I}_{m\nu_a\nu_c,m'\nu_b\nu_d}$, is written simply in the HO basis as

$$\mathcal{I}_{m\nu_a\nu_c,m'\nu_b\nu_d} = \langle m\nu_a m'\nu_b|G(r)F[\rho]|m'\nu_d m\nu_c\rangle = \sum_{\nu_\mu\nu_{\mu'}} T^{\nu_\mu}_{m\nu_a,m'\nu_d}\, T^{\nu_{\mu'}}_{m'\nu_b,m\nu_c}\langle 00,00|G|m' - m\nu_\mu, m - m'\nu_{\mu'}\rangle. \tag{16}$$

The analytical expression of the quantities T appearing in Eq. (16) are given in Appendix B by Eq. (B43). The expression of the quantity $\langle 00,00|G|r_\mu,r_{\mu'}\rangle$ is

$$\langle 00|G|r_\mu r_{\mu'}\rangle = \frac{\delta_{m_\mu+m_{\mu'},0}\ \ \beta_\perp p^2}{(2+\beta_\perp p^2)^{n_{\perp\mu}+n_{\perp\mu'}+|m_\mu|+1}} \frac{(n_{\perp\mu}+n_{\perp\mu'}+|m_\mu|)!}{[n_{\perp\mu}!\,(n_{\perp\mu}+|m_\mu|)!\ n_{\perp\mu'}!\,(n_{\perp\mu'}+|m_{\mu'}|)!]^{1/2}} \times \frac{(-)^{(n_{z\mu}-n_{z\mu'})/2}\ p\sqrt{\beta_z}}{(2+\beta_z p^2)^{(n_{z\mu}+n_{z\mu'}+1)/2}} \frac{(n_{z\mu}+n_{z\mu'})!}{[(n_{z\mu}+n_{z\mu'})/2]!}\sqrt{\frac{2^{-n_{z\mu}-n_{z\mu'}}}{n_{z\mu}!\ n_{z\mu'}!}}, \tag{17}$$

where the first line corresponds to the radial matrix element and the second to the z matrix element.

The expression (13) of the first term of the exchange field becomes

$$\Gamma\,[1]^{q\Omega=m+s}_{m\nu_a,m\nu_c}(E) = \sum_{m'\geqslant 0\nu_b\nu_d} \mathcal{I}_{m\nu_a\nu_c,m'\nu_b\nu_d} R^{qs}_{m'\nu_d\nu_b}. \tag{18}$$

The quantity $\mathcal{I}_{m\nu_a\nu_c,m'\nu_b\nu_d}$ is independent of the density matrix ρ and is calculated once and for all at the beginning of the code. However, the field term $\Gamma\,[1]^{q\Omega=m+s}_{m\nu_a,m\nu_c}(E)$ has to be recalculated at each iteration as it depends on the one-body density ρ through the quantity $R^{qs}_{m'\nu_d\nu_b}$. In the calculation of this field term, the summation is numerically achieved by loops on the indices m', ν_b, and ν_d. These loops are themselves inserted in another loops on m, ν_a, ν_c, q, and s. Apart from the spin s and isospin q indices, the other indices describe a set of values limited by the size of the HO basis whose size is N_0.

2. Case 2: $G(r) = e^{-r^2/p^2}$ and $F[\rho] = \frac{1}{2}[\rho^\alpha(\vec{r}_1) + \rho^\alpha(\vec{r}_2)]$

In the present case, the full expression of the interaction takes the form

$$\widehat{v}_{12} = (W + B\widehat{P}_\sigma - H\widehat{P}_\tau - M\widehat{P}_\sigma\widehat{P}_\tau)e^{-r^2/p^2} \times \frac{\rho^\alpha(\vec{r}_1) + \rho^\alpha(\vec{r}_2)}{2}. \tag{19}$$

From the expression (B56), we deduce the expression of the spatial part of the matrix element,

$$\langle m\nu_a \;\; m'\nu_b|G(r)F[\rho]|m'\nu_d \;\; m\nu_c\rangle = \pi \int d^2\widetilde{r}\;\rho^{\alpha}(\widetilde{r})\big[\phi_{|m|\nu_a}(\widetilde{r})\phi_{|m'|\nu_d}(\widetilde{r})\widetilde{G}_{m'\nu_b,m\nu_c}(\widetilde{r}) + \phi_{|m'|\nu_b}(\widetilde{r})\phi_{|m|\nu_c}(\widetilde{r})\widetilde{G}_{m\nu_a,m'\nu_d}(\widetilde{r})\big], \quad (20)$$

where the function $\phi_{|m|\nu}(\widetilde{r})$ are the HO wave functions defined in Eq. (A6) of Appendix A left without their phase $e^{im\varphi}$ and $\widetilde{r} \equiv (r_\perp, z)$, with $r_\perp$ the projection of $\vec{r}$ on the plane xOy and z its projection along the symmetry axis Oz. The quantities $\widetilde{G}_{m_i\nu_i,m_j\nu_j}(\widetilde{r})$ are defined by Eq. (B54) of Appendix B.

That leads to

$$\Gamma[1]^{q\Omega=m+s}_{m\nu_a,m\nu_c}(E) = \sum_{m'\geqslant 0\;\nu_b\nu_d} \pi \int d^2\widetilde{r}\;\mathcal{J}_{m\nu_a\nu_c,m'\nu_b\nu_d}(\widetilde{r}) \times \rho^{\alpha}(\widetilde{r})R^{qs}_{m'\nu_d\nu_b}. \quad (21)$$

As the quantity $R^{qs}_{m'\nu_d\nu_b}$, the spatial density $\rho(\widetilde{r})$ depends on the one-body density matrix ρ and has to be recalculated at each iteration. Moreover, the integral appearing in Eq. (20) is approximate numerically by a summation on the Laguerre-Gauss and Hermite-Gauss points $\widetilde{r} = (r_\perp, z)$,

$$\int d^2\widetilde{r}\;f(\widetilde{r}) = \int r_\perp dr_\perp dz\;\; f(r_\perp,z) \simeq \sum_{i,j} v_i w_j\, r_{\perp i} e^{r_{\perp i}} e^{z_j^2} f(r_{\perp i}, z_j), \quad (22)$$

where v_i and w_j are the Laguerre-Gauss and Hermite-Gauss weights.

Then the calculation of the term of the field takes the form

$$\Gamma[1]^{q\Omega=m+s}_{m\nu_a,m\nu_c}(E) = \sum_{m'\geqslant 0\;\nu_b\nu_d}\sum_{i,j} \mathcal{L}_{m\nu_a\nu_c,m'\nu_b\nu_d}(r_{\perp i}, z_j) \times \mathcal{R}^{qs}_{m'\nu_d\nu_b}(r_{\perp i}, z_j), \quad (23)$$

where

$$\mathcal{L}_{m\nu_a\nu_c,m'\nu_b\nu_d}(r_{\perp i}, z_j) = \pi\, v_i w_j\, r_{\perp i} e^{r_{\perp i}} e^{z_j^2} \times \mathcal{J}_{m\nu_a\nu_c,m'\nu_b\nu_d}(r_{\perp i}, z_j) \quad (24)$$

and

$$\mathcal{R}^{qs}_{m'\nu_d\nu_b}(r_{\perp i}, z_j) = \rho^{\alpha}(r_{\perp i}, z_j) R^{qs}_{m'\nu_d\nu_b}. \quad (25)$$

Then, at each iteration, the calculation of the field term $\Gamma[1]^{q\Omega=m+s}_{m\nu_a,m\nu_c}(E)$ requires a loop on each index q, s, m, ν_a, ν_c, m', ν_b, ν_d, i, and j. As in Case 1, apart from the spin s and isospin q indices, the other indices describe a set of values limited by the size of the HO basis whose size is N_0.

3. *Computation time of* $\Gamma[1]^{q\Omega=m+s}_{m\nu_a,m\nu_c}(E)$

In this part, we are first interested in evaluating the computation time of an algorithm in which the loops on the various indices are nested and the algebraic operations are done in the most internal loop. Inside the loops, the instruction that builds the summation contains two operations, a multiplication and an addition. By noting as $t[\times]$ the execution time of a multiplication and $t[+]$ the one of an addition, the execution time T_1 of the loops of Case 1 is

$$T_1 = N_1\,(t[\times] + t[+]), \quad (26)$$

with $N_1 = 2 \times 2 \times N_m \times N_{\nu_a} \times N_{\nu_c} \times N_{m'} \times N_{\nu_b} \times N_{\nu_d}$, where the various quantities N_k appearing on the right side of Eq. (26) represent the number of possible values taken by the quantum number k for a given HO basis whose size is N_0.

The execution time T_2 of the loops of Case 2 is

$$T_2 = N_2\,(t[\times] + t[+]), \quad (27)$$

where $N_2 = N_1 \times N_i \times N_j$ and $(N_i,\, N_j)$ are the number of Laguerre-Gauss and Hermite-Gauss points, respectively.

The execution times have been evaluated for the $D1$-type and $D2$ Gogny forces. We note that the execution times of the zero-range terms are so fast that they have been neglected. We deduce that the time T_{D1} corresponding to the $D1$-type Gogny force, for the calculation of the field term $\Gamma[1]^{q\Omega=m+s}_{m\nu_a,m\nu_c}(E)$, can be approximate as

$$T_{D1} \simeq 2T_1. \quad (28)$$

With the new analytical form $D2$ of the Gogny force, this time, noted T_{D2}, is evaluated as

$$T_{D2} = 2T_1 + T_2 = (2 + N_i N_j)T_1 = \left(1 + \tfrac{1}{2}N_i N_j\right) T_{D1}. \quad (29)$$

In a case of spherical nuclei, the dependence $N_i{=}N_j{=}2N_0$, which is a realistic prescription for the evaluation of the integrals, has been chosen for the numbers N_i and N_j of Laguerre-Gauss and Hermite-Gauss points.

The execution times T_{D1} and T_{D2} of one iteration are indicated in Table V, according to the size N_0 of the HO basis. We see that the execution time T_{D2} is excessively larger than T_{D1} (up to a factor $\sim$649 for $N_0 = 18$) when a naive program writing is done.

TABLE V. Computation time (in seconds) of one iteration of the AMEDEE HFB code, according to the size N_0 of the HO basis. Calculations have been done on a standard computer using one processor.

N_0	4	6	8	10	12	14	16	18
T_{D1}	0.003	0.011	0.056	0.167	0.494	1.212	2.976	8.616
T_{D2}	0.099	0.803	7.224	33.50	142.9	476.4	1527	5592
T'_{D2}	0.012	0.068	0.309	1.087	3.218	8.741	17.31	36.04
$\frac{T_{D2}}{T_{D1}}$	33	73	129	201	289	393	513	649
$\frac{T'_{D2}}{T_{D1}}$	4.0	6.2	5.5	6.5	6.5	7.2	5.8	4.2

To improve in a significant way T_{D2}, we have proposed a restructuring of the loops. To explain this restructuring, we start with a simple example to understand its main idea. We consider the following quantity s that is to be calculated from functions f_i which depend on indices (a,b,c) in the following way:

$$s = \sum_{a=1}^{N}\sum_{b=1}^{N}\sum_{c=1}^{N} f_1(a)\, f_2(a,b)\, f_3(b,c). \quad (30)$$

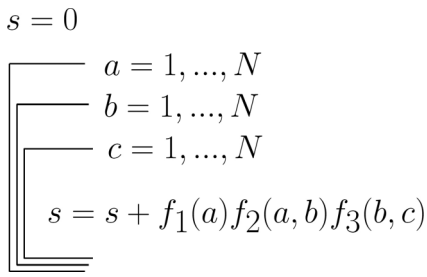

FIG. 8. The simplest loop structure to calculate s (see text).

As seen from Eq. (30), the functions f_i are assumed to be linked by common indices.

From a numerical point of view, the multiple summation (30) is programmed as a set of nested loops. There are several ways of organizing these loops; some are more time expensive. The simplest loop structure is represented on Fig. 8. Inside the loops, three mathematical operations are achieved: two multiplications and one addition. The corresponding execution time T_s is thus

$$T_s = N^3 \left(2t[\times] + t[+]\right), \tag{31}$$

where N is the number of values taken by the three indices (a,b,c).

To show that there exists a loop structure which reduces the number of mathematical operations, we use a graphical representation whose prescription can be defined in the following way. The quantity s contains a summation on the set of indices (a,b,c). These indices are linked by functions; for example, the function $f_2(a,b)$ correlates the indices a and b. Consequently, these functions make up indivisible blocks, $f_2(a,b) \neq f_{2.a}(a).f_{2.b}(b)$, which can be represented by points. Moreover, these various functions are connected between themselves by their common indices. We represent a connection between two functions with a line labeled by their common index. Using this graphical prescription, the representation of the quantity s is shown on Fig. 9.

The following step consists of determining the index of the summation that have to be achieved first. In the present simple case, we see the following.

(i) The summation on the index a is related to the functions $f_1(a)$ and $f_2(a,b)$. Two loops are necessary, one on the index a that is summed up and the other on the spectator index b.

(ii) The summation on the index b is related to the functions $f_2(a,b)$ and $f_3(b,c)$. Three loops are necessary, one on the index b that is summed up and two on the spectator indices a and c.

(iii) The summation on the index c concerns only the function $f_3(b,c)$. Two loops are necessary, one on the index c that is summed up and the other on the spectator index b.

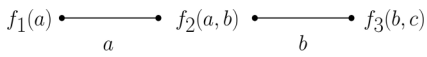

FIG. 9. Graphical representation of the quantity s (see text).

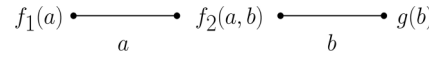

FIG. 10. Graphical representation of the quantity s (see text).

This small analysis shows that it is not advantageous to do the summation on b first. Concerning the summations on the indices a and c, the graphical representation shown in Fig. 9 allows us to conclude that the first summation that we have to do is the one on c. Indeed, a linked is labeled by the index a, which is not the case for the index c. This link represents the multiplication between the functions $f_1(a)$ and $f_2(a,b)$. This multiplication, which is time expensive, discriminates the summation on the index a. The summation on c implies the definition of the function $g(b) = \sum_c f_3(b,c)$. With this presummation, the new expression for s is $s = \sum_{a,b} f_1(a) f_2(a,b) g(b)$. The corresponding graphical representation is given on Fig. 10. The new graph (10) shows that indices a and b see the same type of environment: one function with one variable, one function with two variables and one link. Hence, the summation on a and b are equivalent from the point of view of the execution time. For example, if we choose to do first the summation on b, s can be written as $s = \sum_a f_1(a) h(a)$, with $h(a) = \sum_b f_2(a,b) g(b)$.

The final structuring of the loops is shown on Fig. 11. Within this new loop structuring, the presummation calculation $g(b)$ corresponds to N^2 additions. The second pre-summation $h(a)$ gives rise to N^2 multiplications and the same number of additions. Hence, the execution time $T_s^{'}$ of this new loop structuring is

$$T_s^{'} = N^2 t[+] + N(N+1)(t[\times] + t[+]). \tag{32}$$

From a numerical point of view, $t[+] \ll t[\times]$. Then we obtain for T_s and $T_s^{'}$

$$\left.\begin{array}{l} T_s = 2N^3\, t[\times] \\ T_s' = N(N+1)\, t[\times] \end{array}\right\} \Rightarrow T_s' \leqslant T_s \quad \text{for all} \quad N \geqslant 1. \tag{33}$$

We have used the same reduction procedure for the calculation of the various fields appearing in the HFB equations.

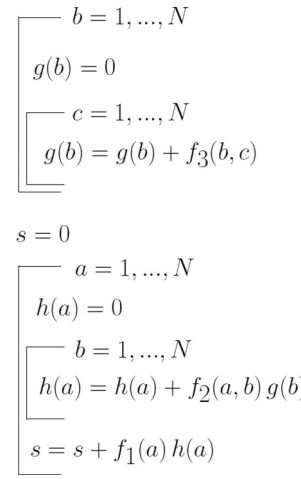

FIG. 11. Structuring of the loops that optimizes the execution time of the quantity s (see text).

For the quantity $\Gamma[1]^{q\Omega=m+s}_{mv_a,mv_c}(E)$, the situation is much more complicated than in the previous example because they are much more indices and different functions. The final ordering of the loops (external to internal) that is obtained is $\sum_i$, $\sum_j$, $\sum_{m'>0,n_{\perp b}}$, $\sum_{v_b}$, $\sum_{m'>0,n_{\perp d}}$, and $\sum_{v_d}$. The execution times T'_{D_2} are indicated in Table V. We see that the increase of the execution time owing to the finite-range, density-dependent term is equal now to only a factor ranging from 4.0 to 7.2, depending on the size N_0 of the HO basis. The restructuring of the loops makes the HFB code with the $D2$ interaction still very competitive in time.

B. Tin isotopic chain

1. Spin of odd isotopes

The ground states and excited states of many odd Sn isotopes have been produced experimentally. In Fig. 12, we report their measured spin, parity, and excitation energies (EXP) extracted from the ENSDF data base of the National Nuclear Data Center [82]. The predictions of our HFB calculations (without breaking of time-reversal symmetry), using the $D1S$ and $D2$ parametrizations, are also presented for 11 odd isotopes, ranging from ^{111}Sn to ^{131}Sn (the $D2A$ parametrization is similar to the $D2$ parametrization but differ by a stronger surface pairing). They are all found to be spherical.

For ^{111}Sn, the results with the two parametrizations predict the spin parity $7/2^+$ for the ground state, in agreement with the experiment. Until ^{119}Sn, the measured spin parities $1/2^+$ of the ground state and the first two excited states are correctly reproduced by the Gogny parametrizations (no experimental spin and parity are available for the second excited states in ^{111}Sn and ^{113}Sn). The ^{121}Sn is the first isotope for which the theoretical predictions do not reproduce the measured spin parity $3/2^+$ for the ground state. It is still possible that the particle-vibration coupling induces a permutation of the $1/2^+$ and $3/2^+$ states, for they are very close in energy. In ^{123}Sn, the measured ground state has a spin parity $11/2^-$, correctly reproduced with the $D1S$ parametrization. The $D2$ parametrization fails to reproduce this spin-parity and still predicts the ground state as $1/2^+$. In the isotopes ^{129}Sn and ^{131}Sn, the experimental spectra are built on a $3/2^+$ ground state. The predictions of the $D1S$ and $D2$ parametrizations fail to reproduce the spin parity of the ground state. They predict a $11/2^-$ ground state.

To conclude, excitation energies obtained within a self-consistent blocking of the HFB approach are in general found in better agreement with the $D2$ parametrization than the $D1S$ parametrization, even though noticeable disagreement is found around the $N = 82$ shell closure. Moreover, we remark that the desired accuracy of the theoretical predictions has to be of the order of $\sim$100 keV, or even less, to reproduce the experimental spectra for the heavier isotopes. The difference

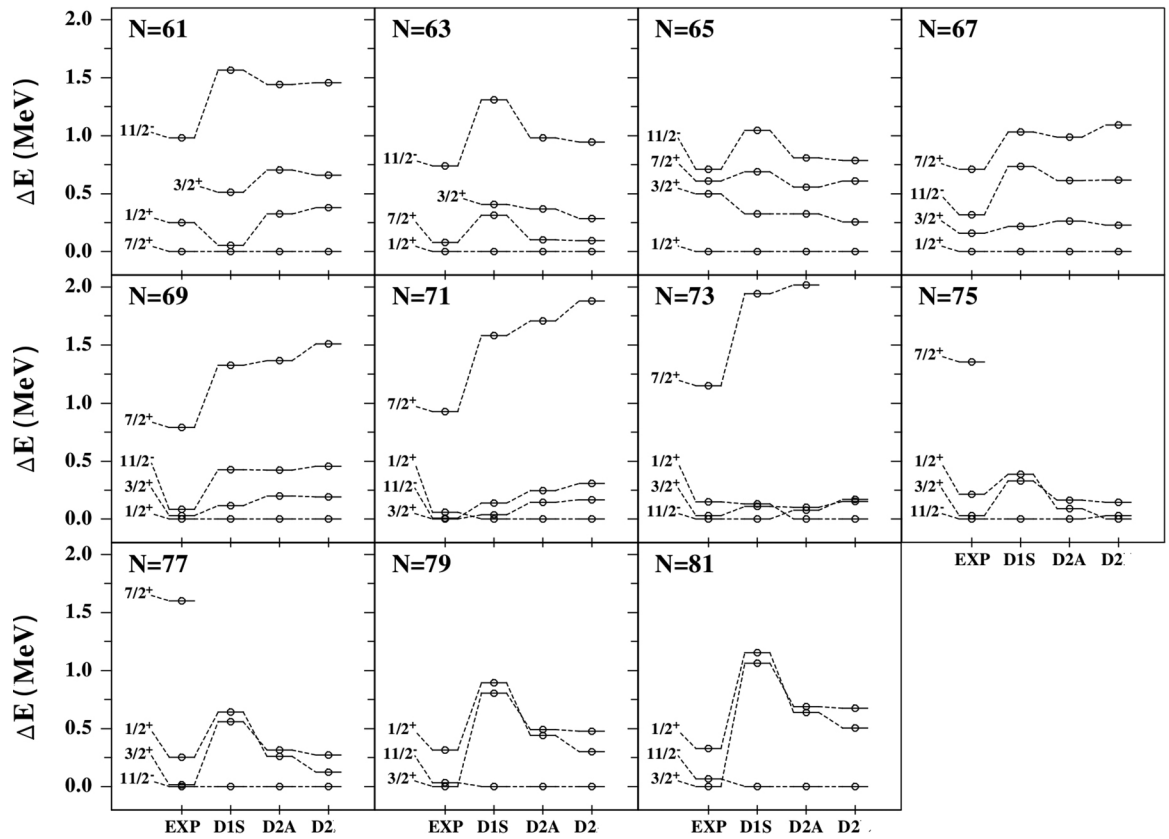

FIG. 12. Spin, parity, and excitation energies $\Delta(E)$ (in MeV) of the ground and the first excited states in 11 odd Sn isotopes, with a number of neutron ranging from 61 to 81. Experimental results as well as the predictions of the $D1S$ and $D2$ parametrizations are indicated. The $D2A$ parametrization is similar to the $D2$ parametrization but differs by a stronger surface pairing.

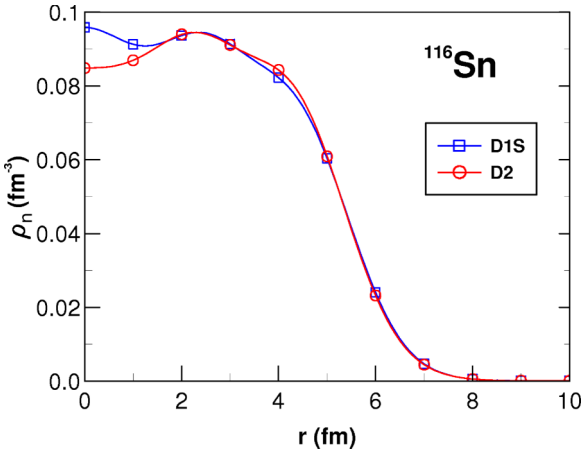

FIG. 13. (Color online) Spatial distribution of the neutron density in the ^{116}Sn isotope calculated with the $D1S$ (empty squares) and the $D2$ (empty circles) parametrizations.

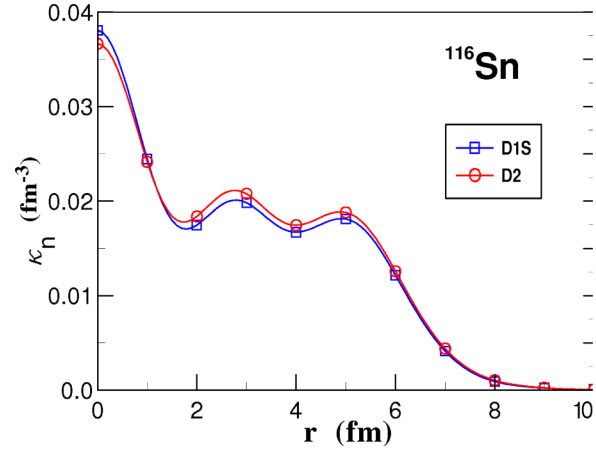

FIG. 14. (Color online) Spatial distribution of the correlated neutron pairs $\kappa_n(r)$ in the ^{116}Sn isotope, calculated with the $D1S$ (empty squares) and the $D2$ (empty circles) parametrizations.

in energy between the HFB calculations and the experiment is consistent with the magnitude of the particle-vibration effect in odd nuclei [17,83].

2. *Spatial distribution of nucleons and correlated pairs*

The spatial distribution of nucleons with isospin τ (proton or neutron) is characterized by the local density $\rho_\tau(\vec{r})$ defined by

$$\rho_\tau(\vec{r}) = \sum_{i,j,\sigma} \phi_i^*(\vec{r},\sigma,\tau)\phi_j(\vec{r},\sigma,\tau)\rho_{ji}, \tag{34}$$

where $\vec{r}$, σ, and τ denote the position, the spin, and the isospin; $\phi_i(\vec{r},\sigma,\tau)$ the wave function of the state i in a given representation; and ρ_{ij} the density matrix.

In Fig. 13, the neutron local density $\rho_n(\vec{r})$ calculated within the HFB approach is displayed in the case of ^{116}Sn for both the $D1S$ (empty squares) and the $D2$ (empty circles) parametrizations. As this nucleus is spherical, the density is isotropic and depends only on the norm r of the position $\vec{r}$. Moreover, the structure of the local density is given by the spatial form of the single-particle orbitals that are filled or partially filled. One observes that the neutron local density is very similar for large values of r ($r > 5$ fm) for the two parametrizations. Differences appear in the center and in the surface of the nucleus. The largest difference is found in the center where, a depression is obtained for the $D2$ parametrization. This difference comes from the filling of s states that are the only ones to contribute to the density in the center of the nucleus.

To further interpret this difference, we have investigated the spatial distribution of the neutron correlated pairs. In the HFB approach, this distribution is characterized by the pairing tensor $\kappa_\tau(\vec{r})$:

$$\kappa_\tau(\vec{r}) = \sum_{i,j,\sigma} \phi_i(\vec{r},\sigma,\tau)\phi_j(\vec{r},\sigma,\tau)\kappa_{ji}. \tag{35}$$

It is known that only the states i and j close to the Fermi level contribute significantly to the pairing tensor [84,85]. The spatial distribution of the neutron correlated pairs $\kappa_n(r)$ in ^{116}Sn is shown on Fig. 14 for both the $D1S$ (empty squares) and $D2$ (empty circles) parametrizations. One observes that the main differences between the two parametrizations occur for the same value of r as observed in the neutron density $\rho_n(r)$. For ^{116}Sn, the neutron chemical potential is located between the $3s_{1/2}$ and the $2d_{3/2}$ single-particle states. Clearly, the difference obtained for the neutron local density in the center of the nucleus arises from the $3s_{1/2}$ orbital that is less populated with the $D2$ parametrization than with the $D1S$ parametrization. The pairing correlations are accountable for these results. The fluctuations around the surface ($r \sim 4$ fm) come mainly from the $2d_{3/2}$, which is more filled with the $D2$ parametrization than in the case of the $D1S$ parametrization. This result shows that the pairing strength of the $D2$ parametrization is a bit stronger than the $D1S$ parametrization (more surface pairing). It is consistent with the pairing gap curve (Fig. 7) found in nuclear matter. From these results, it is difficult to discriminate between different parametrizations. Indeed, concerning the neutron density profile in ^{116}Sn, no experimental data are known.

3. *Odd-even mass difference*

The odd-even mass difference is the pertinent observable to quantify the pairing correlations in nuclei. Indeed, it has been identified at the beginning of nuclear physics [86] and explained through the existence of pairing correlations between the nucleons [87]. Different studies [88,89], based on the microscopic analysis of the mean-field and pairing-field contributions, have shown that the three-point mass difference $\Delta^{(3)}(A)$, centered on an odd nucleus, gives an estimation of the pairing gap magnitude. This difference is defined as

$$\Delta^{(3)}(A) = \frac{(-1)^A}{2}\left[E(A+1) - 2E(A) + E(A-1)\right], \tag{36}$$

where $E(A-1)$, $E(A)$, and $E(A+1)$ represent the binding energies of the systems with $A-1$, A, and $A+1$ nucleons, respectively.

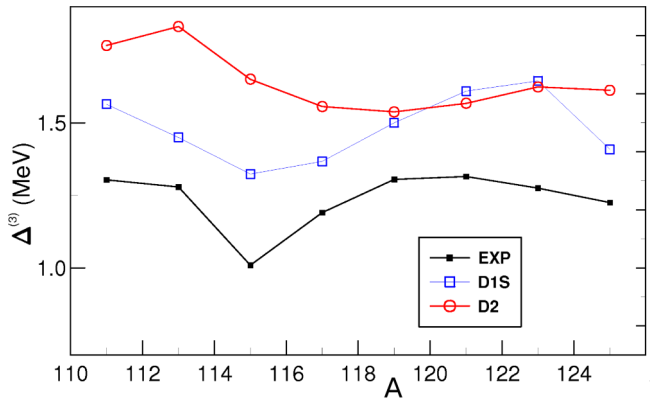

FIG. 15. (Color online) Odd-even mass difference $\Delta^{(3)}$ according to the number of nucleons A in the Sn isotopic chain. The results are shown for the $D1S$ (empty squares) and $D2$ (empty circles) parametrizations and compared to the experimental data (EXP) (solid squares).

In Fig. 15, the values of $\Delta^{(3)}(A)$ calculated at the HFB approximation with the blocking prescription [90] for the odd nuclei, are compared with the experimental values (solid squares) [91]. The theoretical curve obtained with the $D1S$ parametrization (empty squares) reproduces correctly the shape of the experimental curve. Especially, it has a minimum at $A = 115$, in agreement with the experimental curve. This minimum is linked to the decrease of the pairing correlations at the shell closure $1g_{7/2}$ in ^{114}Sn. With the $D2$ parametrization (empty circles), the minimum of the mass differences $\Delta^{(3)}(A)$ is postponed to $A = 119$. However, these results do not include the residual interaction effects beyond the mean field, such as the particle-vibration coupling, that are known to be important especially in odd nuclei. To leave room to treat explicitly these particular correlations, the Gogny interaction is fitted to provide odd-even mass differences in Sn isotopes larger than the experimental values. Originally, Gogny estimated that the effect of the particle-vibration coupling is of the order of ~300 keV [17,83]. This value is still in use in the fitting procedure.

To compare the pairing strength of the two different parametrizations, we have displayed in Fig. 16 the neutron pairing energy E_{app} in the even-even Sn isotopes ranging from $A = 100$ to $A = 138$. As already noticed in the nuclear-matter pairing study, the neutron pairing energy is systematically found to be a bit stronger with the $D2$ parametrization than with the $D1S$ parametrization.

C. Lead isotopic chain

1. Charge and neutron distributions in ^{208}Pb

The role played by the $3s_{1/2}$ orbital can be studied through the charge distribution in ^{208}Pb, as it is located in the proton Fermi sea in this nucleus. In Fig. 17, bottom curves, the charge distributions are represented for the $D1S$ (empty squares) and the $D2$ (empty circle) parametrizations. They have been calculated at the HF approximation and taking into account the proton form factor. Results deduced from a RPA calculation with the $D1S$ parametrization as well as the experimental data are also indicated.

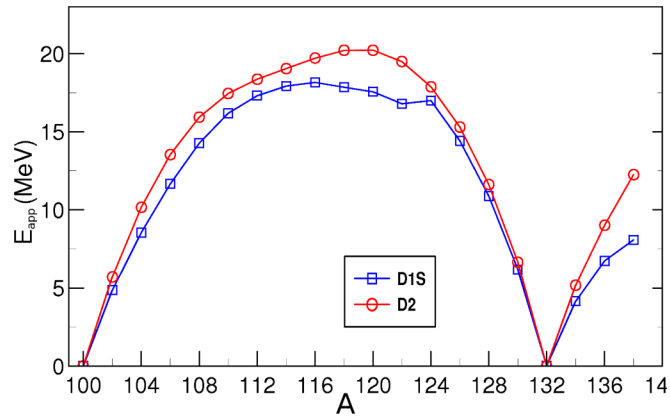

FIG. 16. (Color online) Neutron pairing energy E_{app} (in MeV) of a few Sn isotopes, calculated with the $D1S$ (empty squares) and $D2$ (empty circles) parametrizations.

For the $D1S$ parametrization, the charge distribution obtained with the HF method reproduces reasonably well the experimental data (EXP) beyond $r = 2$ fm. Indeed, at the level of the HF approximation, it is not expected to reproduce such experimental data with the Gogny interaction. In the center of the nucleus, $r < 2$ fm, the HF calculation is different from the experimental curve by predicting a too-pronounced maximum. This maximum at the origin [$\rho(0) = 0.077$ fm^{-3}] comes from the contribution of the $3s_{1/2}$ and overestimates the experimental value [$\rho(0) = 0.063$ fm^{-3}]. The adding of correlations in the ground state using the RPA method improves significantly the agreement with the experimental distribution. The discrepancy to experiment is reduced by a factor of 2 [92,93].

For the $D2$ parametrization, only calculations at the HF level are discussed. In comparison with the $D1S$ parametrization, the value at the center of the nucleus is reduced by 0.002 fm^{-3}. This slight improvement of the theoretical results

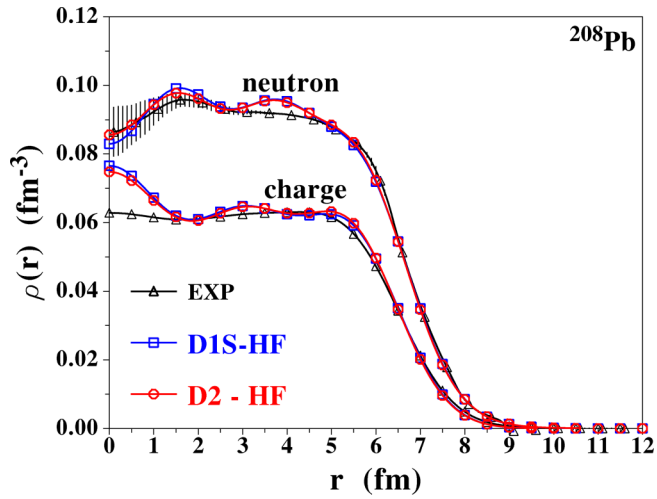

FIG. 17. (Color online) Spatial distribution of the neutron density in the ^{208}Pb isotope calculated with the $D1S$ (empty squares) and the $D2$ (empty circles) parametrizations.

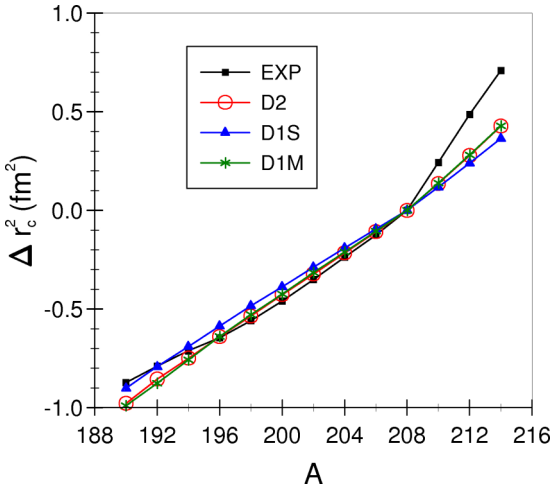

FIG. 18. (Color online) Isotopic variation of charge radii Δr_c^2 for the Pb isotopes according to the mass A. The theoretical prediction obtained at the HFB approximation for the $D1S$, $D1M$, and $D2$ parametrizations are compared to the experimental ones (EXP).

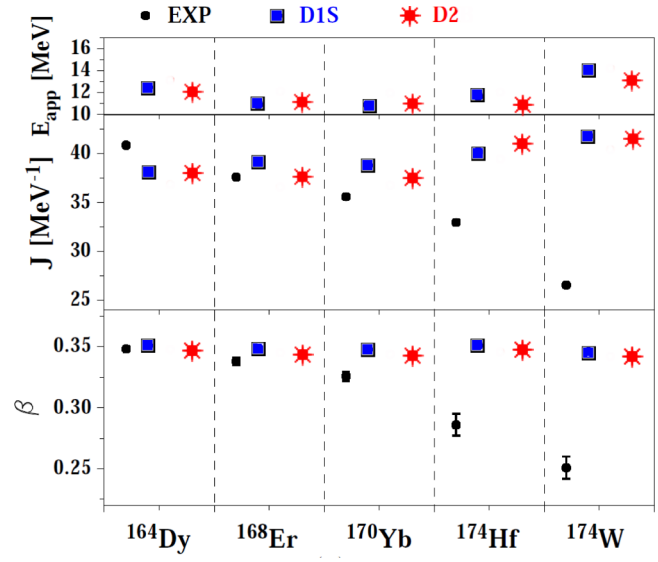

FIG. 19. (Color online) (Top) Pairing energy calculated at the HFB approximation. (Middle) Moments of inertia. (Bottom) Axial deformation β. Calculations have been done for a few nuclei of the rare-earth region with the $D1S$ (blue) and $D2$ (red) parametrizations. Experimental data are indicated with black points.

obtained at the HF level goes in the right direction. It would be very interesting to complete this calculation with a RPA one.

The neutron distribution is experimentally less easily determined, in particular in the center of the nucleus. In Fig. 17, top curves, the neutron densities (experimental and theoretical) are displayed. The experimental error bars are represented by vertical black lines. In the central region, $r < 3$ fm, the distribution obtained with the $D1S$ parametrization at the HF and HF-RPA approximations displays oscillations with an amplitude that is slightly too strong according to the experimental value. With the $D2$ parametrization, the amplitude is reduced and the distribution obtained at the HF approximation is compatible with the error bars.

2. *Isotopic variation of charge radii*

The isotopic variation of charge radii is a stringent test of our theoretical models. The experimental values, deduced from spectroscopy with Laser beam, are known with a high accuracy along isotopic chains [94,95]. In the Pb isotopic chain, the experimental charge radii display an angular point at the ^{208}Pb isotope. This effect can be seen in Fig. 18 where the quantity Δr_c^2 defined as

$$\Delta r_c^2 = r_c^2(A) - r_c^2(208) \tag{37}$$

has been plotted. In expression (37), $r_c(A)$ is the charge radius of the isotope of mass A. For all the curves, the reference point is ^{208}Pb. The curve denoted EXP corresponds to experimental charge radii. For the other curves, the charge radii have been calculated at the HFB approximation using the $D1S$ [35], $D1M$ [49], and $D2$ parametrizations. The predictions for $D1M$ and $D2$ are very similar.

The $D1S$ parametrization predicts a negligible changing of slope. A slight improvement is obtained with the $D2$ and $D1M$ parametrizations. Moreover, we remark that, for the isotopes with mass $A < 208$, the $D2$ and $D1M$ parametrizations reproduce with a very good accuracy the experimental isotopic variation of the charge radii up to ^{196}Pb. For the lightest isotopes ($^{190-194}$Pb), collective beyond-mean-field correlations begin to play a role. Indeed, Ref. [51] shows clearly that these isotopes are no longer rigid. This effect is confirmed by the changing of slope on the experimental curve before ^{196}Pb. From other studies (relativistic and nonrelativistic) [26,96,97], it seems that the isovectorial component of the spin-orbit term may play a role for a better agreement with the experimental kink. The actual spin-orbit term of the Gogny interaction is a contact term and acts only in the odd-triplet channel ($S = 1$, $T = 1$). Its isovectorial dependence is very particular. Adding a finite range to this component would allow a contribution in the even-triplet channel ($S = 1$, $T = 0$).

D. Moments of inertia in rare-earth and actinide regions

In rare-earth and actinide regions, low-energy collective states of many even-even nuclei have been experimentally produced. The energies of the first excited states built on the 0^+ ground state have been measured. The first excited state, in most even-even nuclei, has spin parity 2^+. The experimental values of the excitation energy for this state, $E(2^+)$, are compiled in Ref. [98].

The axial deformation β of the ground states of a few rare-earth and actinide nuclei are displayed in Figs. 19 and 20, bottom panels. The experimental deformations are indicated with solid circles whereas the theoretical results obtained at the HFB approximation correspond to solid squares ($D1S$ parametrization) and stars ($D2$ parametrization). As is well known, the experimental results are characterized by the occurrence of strong axial deformations, with a β deformation ranging typically from 0.25 to 0.35. Except for ^{174}Hf and ^{174}W, for which the HFB theory overestimates experiment,

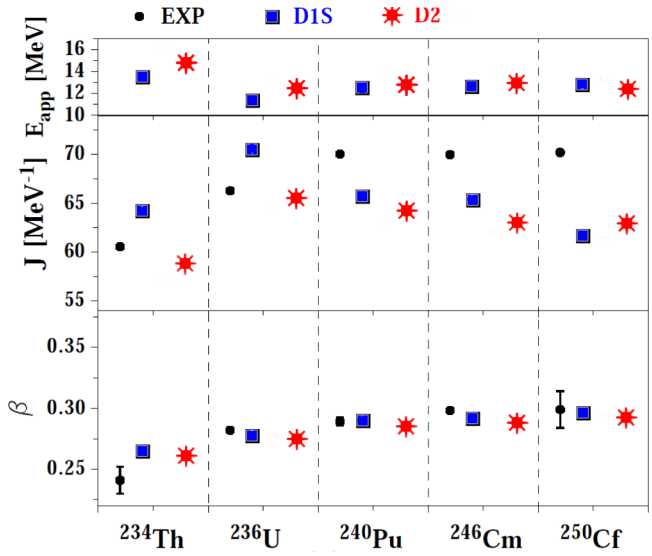

FIG. 20. (Color online) Same as Fig. 19 for a few actinides.

the theoretical predictions, done at the HFB level, provide a deformation β in good agreement with the experimental data.

As a consequence of the strong experimental deformation in the two mass regions, the first excited states follow a rotational spectrum law. Thus, the experimental values of the moment of inertia can be deduced from the measured energy of the first 2^+ state, as $J_{\rm EXP} = 3/E(2^+)$ (MeV^{-1}). The experimental moments of inertia are represented with black circles in Figs. 19 and 20, middle panel. The theoretical predictions obtained with the $D1S$ and $D2$ parametrizations (blue and red points, respectively) have been calculated at the Inglis-Belyaev [99,100] approximation, following the procedure proposed by Girod *et al.* [101] to reproduce the values deduced from the Thouless-Valatin method [102].

For the rare earths ^{164}Dy, ^{168}Er, and ^{170}Yb, the calculated moments of inertia reproduce correctly the experimental data, with an accuracy of 5 MeV^{-1}. This theory-experiment agreement is much worse in ^{174}Hf and ^{174}W, as for the deformation β. Experimentally, the strong relation between moments of inertia and deformation has been proved and can be parametrized as [90]

$$J_{\rm EXP} \simeq \frac{\beta_{\rm EXP}^2 A^{7/3}}{400} \ ({\rm MeV}^{-1}). \qquad (38)$$

Applying the relation (38) to the theoretical results, the difference $(\beta_{D1S}^2 - \beta_{\rm EXP}^2) = 0.056$ in ^{174}W is equivalent to a difference $(J_{D1S} - J_{\rm EXP}) = 23.7$ MeV^{-1}. Looking at Fig. 19, the difference is, in fact, a little bit smaller (15.3 MeV^{-1}) but still of the same order of magnitude. We note that the two parametrizations provide close results.

Finally, we display in Figs. 19 and 20, top panel, the pairing energy $E_{\rm app}$ obtained for the various isotopes. Both parametrizations show similar pairing contents with the deformation.

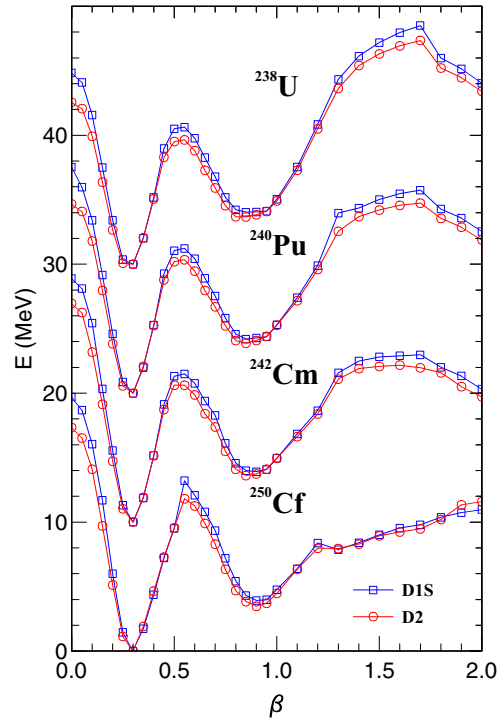

FIG. 21. (Color online) Potential energy evolution $E_{\rm HFB}$ according to the axial quadrupole deformation parameter β for a few actinides (see text). The calculations have been done for the $D1S$ (empty squares) and $D2$ (empty circles) parametrizations. The curves corresponding to the $D2$ parametrization have been translated in order that their minimum correspond to the ones calculated with the $D1S$ parametrization.

E. Fission barriers in actinides

The theoretical modelization of the fission process needs to know both the static and the dynamic properties of the fissioning system. Especially, the static nuclear configurations out of equilibrium, the coupling between collective and single-particle degrees of freedom, as well as the dynamics of the large amplitude collective motions have to be considered. The main microscopic approaches to fission, in particular the one using the Gogny interaction, consists of two steps, a static calculation that determines the potential energy surfaces and the collective inertia, a dynamical calculation based on the static results that describes the time evolution of the system up to scission. In the present work, we discuss only the static step by determining, at the HFB approximation under constraint, the potential energy curves (PECs) of various actinides along the symmetric fission path. Indeed, special attention has to be applied to the height of the fission barriers predicted by an effective interaction.

On Fig. 21, we display the evolution of the PECs obtained for ^{238}U, ^{240}Pu, ^{242}Cm, and ^{250}Cf according to the axial deformation parameter β. For each nucleus, the HFB calculations have been done for the $D1S$ (empty squares) and the $D2$ (empty circles) parametrizations. For the $D2$ parametrization, the PEC has been vertically translated so that its minimum is the same as for $D1S$ parametrization. Furthermore, the zero-point energy rotational corrections have been taken into

TABLE VI. Experimental and theoretical fission barrier heights (expressed in MeV) for nine actinides [103,104]. For the theoretical predictions, the calculations have been done with the $D1S$ and $D2$ parametrizations.

	^{234}U	^{238}U	^{238}Pu	^{240}Pu	^{244}Pu
B_I^{EXP}	4.8	6.3	5.6	6.1	5.7
$B_{I,a}^{D1S}$	8.7	10.6	10.3	11.1	12.2
$B_{I,a}^{D2}$	8.0	9.5	9.4	10.2	9.9
	^{242}Cm	^{244}Cm	^{250}Cf	^{252}Cf	
B_I^{EXP}	6.7	6.2	5.6	5.3	
$B_{I,a}^{D1S}$	11.2	11.4	12.3	10.7	
$B_{I,a}^{D2}$	10.2	10.5	10.8	10.1	

account so that the curves represent the collective potential of the fissioning system. We recall that the $D1S$ interaction was created to have a realistic description of the second barrier that was found to be too high with the original $D1$ parametrization [18,19]. The surface tension of the interaction was then decreased.

The PECs obtained with the $D1S$ and the $D2$ parametrizations have, in general, relatively similar shapes. They display two wells whose minima are located around $\beta \sim 0.3$ and $\beta \sim 0.9$. The two wells, which correspond to the ground state of the system and to the fission isomer, are separated by a first barrier whose height $B_{I,a}$ is measured from the bottom of the first well. In the four presented nuclei, $B_{I,a}$ is found to be smaller by $\sim$1 MeV with the $D2$ parametrization than with the $D1S$ parametrization. More systematic calculations seem to generalize this result in actinides for which this difference ranges between 500 keV and 2 MeV. In Table VI, the experimental fission barrier heights are presented for nine nuclei as well as the theoretical predictions of the $D1S$ and $D2$ parametrizations.

However, a direct comparison between experiment and our theoretical calculations have to be nuanced. On the one hand, the experimental barrier heights are defined according to the ground state of the nucleus. The zero-point energy in the first well is of the order of 500 keV; then the theoretical barrier has to be decreased by the same quantity. On the other hand, the calculation with the $D1S$ parametrization shows that the heights of the triaxial barriers are reduced by 2 to 3 MeV in comparison with the axial values $B_{I,a}$. With these reductions, the heights of the barriers obtained with the $D1S$ parametrizations still overestimate by 1 to 2 MeV the experimental values. The reduced values obtained with the $D2$ parametrization seem to go in the right direction.

V. CONCLUSION

In this work, we have investigated a new analytical form for the Gogny effective interaction by including a finite-range density-dependent term. This generalization is a first step towards a fully finite-range Gogny interaction. Indeed, the use of the effective interaction in mean-field extensions like (Q)RPA and second RPA or, more generally, in methods based on multiparticle-multihole expansions imposes a nonzero-range effective interaction. In such cases, the residual matrix elements have to be well behaved; they have to tend to zero at high transfer momenta.

The parameters of the new Gogny interaction have been adjusted to obtain the $D2$ parametrization. The properties of this parametrization have been investigated in both nuclear matter and finite nuclei at the mean-field level. The $D2$ parametrization displays similar properties than the $D1$-type Gogny parametrizations in nuclear matter. A few properties are even improved, as the behavior of the energy per particle in the ST spin-isospin channels. Because of the presence of the density-dependent term in the pairing channel ($S = 0$, $T = 1$) that has been chosen to be repulsive, the pairing produced by the $D2$ parametrization seems to be a bit stronger and more surface than the one of the $D1S$ parametrization. The presence of the finite range provides a nuclear matter that is much more stable than the $D1$-type parametrizations. The various quantities calculated in finite nuclei at the HFB level with the $D2$ parametrization show that this new Gogny interaction displays properties similar to those of the standard parametrization, owing to the unified set of constraints of the fitting procedure. The $D2$ interaction offers a better description of binding energies along isotopic chains with the removal of the drift of the energies observed for increasing neutron number with the $D1S$ parametrization. The height of the fission barriers seem to be improved, with a decreasing between 500 keV and 2 MeV in actinides. For the other nuclear properties investigated in this study, the $D2$ parametrization gives the same quality of description as the $D1S$ interaction.

The perspectives of the present work are numerous. We cite only a few of them. A beyond-mean-field analysis of the $D2$ parametrization should be completed to test its residual interaction. In this context, the new parametrization should be implemented in RPA, QRPA, second RPA, and configuration mixing methods. A systematic study of the low-lying spectroscopy would be important. An improvement in the description of binding energies is still needed as the one done in the context of the $D1M$ interaction. The properties associated with the proton-neutron pairing are also a very interesting and possibly relevant as the density-dependent term that acts in the $ST = 10$ channel is now with a finite range. The generalization of the spin-orbit component of the Gogny interaction with a finite-range term has to be done in a similar way, with a complete refit of the interaction.

ACKNOWLEDGMENT

One of the authors (N.P.) would like to thank D. Peña-Arteaga for various discussions concerning the Landau parameters.

APPENDIX A: THE AXIAL HARMONIC OSCILLATOR REPRESENTATION

We denote $|a\rangle$ as the axial HO states with $a = (\alpha_a, r_a)$, $\alpha_a = (q_a, s_a)$, and $r_a = (m_a, \nu_a) \equiv (m_a, n_{\perp a}, n_{za})$. The quantum numbers q_a and s_a are the projections of the isospin and the intrinsic spin. The quantities n_{za} and $n_{\perp a}$ represent the number of quanta on the symmetry z axis and on the perpendicular direction. By definition, the states $|a\rangle$ are eigenstates of j_z

with the eigenvalue $\Omega_a = m_a + s_a$. By noting

$$\begin{aligned}\overline{a} &= (\overline{\alpha}_a,\overline{r}_a) = (q_a,-s_a,-m_a,\nu_a)\\ &= (q_a,-\Omega_a,-m_a,\nu_a),\end{aligned} \tag{A1}$$

the states $|a\rangle$ and $|\overline{a}\rangle$ correspond by the time-reversal operator $\widehat{T}$:

$$\begin{aligned}\widehat{T}|a\rangle &= \sigma_a|\overline{a}\rangle, \quad \widehat{T}|\overline{a}\rangle = -\sigma_a|a\rangle,\\ \widehat{T}^+|a\rangle &= -\sigma_a|\overline{a}\rangle, \quad \widehat{T}^+|\overline{a}\rangle = \sigma_a|a\rangle, \quad \sigma_a = 2s_a.\end{aligned} \tag{A2}$$

We denote as $a > 0$ the states with $\Omega_a > 0$ and as $a < 0$ those having $\Omega_a < 0$. We write c_a^+ as the operator associated with the state $|a\rangle$ in second quantization and $\overline{c_a^+}$ as its time reversal. The relations (A2) are then equivalent to

$$\begin{aligned}\overline{c_a^+} &\equiv \widehat{T}c_a^+\widehat{T}^+ = \sigma_a c_{\overline{a}}^+, \quad \widehat{T}c_{\overline{a}}^+\widehat{T}^+ = -\sigma_a c_a^+,\\ \widehat{T}^+c_a^+\widehat{T} &= -\sigma_a c_{\overline{a}}^+, \quad \widehat{T}^+c_{\overline{a}}^+\widehat{T} = \sigma_a c_a^+.\end{aligned} \tag{A3}$$

The states of the axial HO are eigenstates of the parity $\widehat{P}$ with the eigenvalues $\pi_a = (-)^{m_a+n_{za}}$:

$$\widehat{P}|a\rangle = (-)^{m_a+n_{za}}|a\rangle. \tag{A4}$$

Finally, the wave functions of the axial HO can be written as

$$\Phi_a(\vec{r},\sigma,\tau) = \phi_{r_a}(\vec{r})\ \chi_{s_a}(\sigma)\chi_{q_a}(\tau), \tag{A5}$$

where the functions χ are the standard two-dimensional spinors for spin and isospin degrees of freedom. The spatial wave functions ϕ_{r_a} decompose into two parts (a part related to the z axis and a part related to the perpendicular direction) and can be written as

$$\phi_{r_a}(\vec{r}) = \phi_{m_a n_{\perp a} n_{za}}(\vec{r}) = \phi_{m_a\nu_a}(\vec{r}_\perp,z) = \phi_{m_a n_{\perp a}}(\vec{r}_\perp)\quad \phi_{n_{za}}(z), \tag{A6}$$

where their respective oscillator lengths $\beta_\perp$ and β_z are given by

$$\beta_\perp = \frac{M\omega_\perp}{\hbar} \simeq \frac{\hbar\omega_\perp}{41.47}, \quad \beta_z = \frac{M\omega_z}{\hbar} \simeq \frac{\hbar\omega_z}{41.47}, \tag{A7}$$

with M the nucleon mass.

The explicit expression of the spatial wave functions $\phi_{mn_\perp}(\vec{r}_\perp)$ and $\phi_{n_z}(z)$ appearing in (A6) are

$$\begin{aligned}\phi_{mn_\perp}(\vec{r}_\perp) &= \left(\frac{\beta_\perp}{\pi}\right)^{1/2}\left[\frac{n_\perp!}{(n_\perp+|m|)!}\right]^{1/2} e^{-\frac{1}{2}\beta_\perp r_\perp^2}\\ &\quad\times (r_\perp\sqrt{\beta_\perp})^{|m|}L_{n_\perp}^{|m|}(\beta_\perp r_\perp^2)\, e^{im\varphi},\\ \phi_{n_z}(z) &= \left(\frac{\beta_z}{\pi}\right)^{1/4}\frac{1}{\left(2_z^n n_z!\right)^{1/2}}\, e^{-\frac{1}{2}\beta_z z^2} H_{n_z}(z\sqrt{\beta_z}),\end{aligned} \tag{A8}$$

where the functions $L_{n_\perp}^{|m|}$ and H_{n_z} are the Laguerre and Hermite polynomials, respectively.

APPENDIX B: CONTRIBUTION OF THE FINITE-RANGE AND DENSITY-DEPENDENT TERM OF THE *D2* GOGNY INTERACTION TO THE HARTREE-FOCK-BOGOLIUBOV FIELDS

In this Appendix, we first recall the basics of the HFB method to introduce the various fields appearing in the formalism and to specify our notations. Then, only the part of the mean-field Γ that is necessary for the discussion of the Sec. IV A will be detailed.

1. Basics of the Hartree-Fock-Bogoliubov method

The HFB ground state $|\widetilde{0}\rangle$ of a system is described by an antisymmetrized product of independent quasiparticle (qp) wave functions,

$$|\widetilde{0}\rangle = \prod_\mu \xi_\mu|0\rangle, \tag{B1}$$

where $|0\rangle$ is the particle vacuum. The set of ξ_μ are the qp operators is defined by

$$\xi_\mu = \sum_a (U_{\mu a}c_a + V_{\mu a}\overline{c_a^\dagger}). \tag{B2}$$

The operators $(c_a^\dagger,\ c_a)$ represent creation and annihilation operators of one particle in the state a. The operators $\overline{c_a^\dagger}$, $\overline{c_a}$ are the time-reversal operators obtained from the operators $c_a^\dagger$, c_a. The quantities $U_{\mu a}$, $V_{\mu a}$ are the coefficients of the transformation between particle and qp operators (B2). Moreover, the HFB ground state is taken as a direct product of a proton by a neutron wave function. Here only the pairing between like particles is considered.

In the present work, we assume that the HFB ground state $|\widetilde{0}\rangle$ is invariant by rotation around the symmetry axis Oz (axial symmetry), invariant by time reversal $\widehat{T}$, potentially invariant by parity $\widehat{P}$, and invariant by reflection according to the plane xOz, i.e., by $\widehat{\Pi}_2 = \widehat{P}\widehat{R}_y(\pi)$. Under these symmetries, the qp states ξ_μ^+ are eigenstates of $\widehat{t}_z$, $\widehat{j}_z$, and potentially $\widehat{P}$. Thus, we write $\mu = (q,\Omega,n)$ and

$$\xi_\mu^+ = \xi_{q\Omega n}^+, \tag{B3}$$

where q and Ω are the eigenvalues of $\widehat{t}_z$ and $\widehat{j}_z$ and n is the number that distinguishes the qp's with the same q and Ω. Moreover, the action of $\widehat{T}$ on the ξ_μ^+ is assumed to have the form

$$\overline{\xi_{q\Omega n}^+} \equiv \widehat{T}\xi_{q\Omega n}^+\widehat{T}^+ = (-)^{1/2-\Omega}\xi_{q-\Omega n}^+. \tag{B4}$$

Considering the previous properties, we expand the qp states on the axial HO states (see Appendix A):

$$\xi_{q\Omega n} = \sum_{r_a}\left(U_{n,r_a}^{q\Omega}c_{q\Omega r_a} + V_{n,r_a}^{q\Omega}\overline{c_{q\Omega r_a}^+}\right). \tag{B5}$$

The summation on $r_a = (m_a,\nu_a)$ is limited to the values $m_a = \Omega \pm 1/2$ (and potentially to the values that conserves parity). The U and V represent real matrices. In double representation, the Bogoliubov-Valatin transformation (B5) writes

$$\begin{pmatrix}\xi_\mu\\ \xi_\mu^+\end{pmatrix} = \sum_a \begin{pmatrix}U & V\\ -V & U\end{pmatrix}_{\mu a}\begin{pmatrix}c_a\\ c_a^+\end{pmatrix}. \tag{B6}$$

The matrix

$$B = \begin{pmatrix} U & V \\ -V & U \end{pmatrix}$$

is orthogonal, which implies the following relations:

$$U^T U + V^T V = \mathbb{I}, \quad U^T V - V^T U = \mathbb{O}. \tag{B7}$$

The U and V matrices are solutions of the HFB equations

$$\begin{pmatrix} h & \Delta \\ -\Delta^* & -h^* \end{pmatrix} \begin{pmatrix} U_\mu \\ V_\mu \end{pmatrix} = E_\mu \begin{pmatrix} U_\mu \\ V_\mu \end{pmatrix}, \tag{B8}$$

where $h_{ac} = K_{ac} - \lambda + \Gamma^{(\mathrm{tot})}_{ac}$ is the mean field with a kinetic component (K_{ac}), a Lagrange parameter λ to ensure the preservation of the mean value of the particle number, and a potential component $\Gamma^{(\mathrm{tot})}_{ac}$. The field Δ is the pairing field and the set of E_μ comprises the qp energies.

The total HFB energy is given by the expression

$$E_{\mathrm{HFB}} = K + V + E_{\mathrm{pair}}, \tag{B9}$$

where

$$K = \sum_{ac} \langle a|\widehat{K}|c\rangle \rho_{ca} \tag{B10}$$

is the kinetic energy,

$$V = \frac{1}{2} \sum_{abcd} \langle ab|\widehat{v}^{(a)}_{12}|cd\rangle \rho_{ca}\rho_{db} \tag{B11}$$

is the potential energy of the mean field, and

$$E_{\mathrm{pair}} = \frac{1}{4} \sum_{abcd} \langle a\overline{c}|\widehat{v}^{(a)}_{12}|b\overline{d}\rangle \sigma_c\sigma_d\kappa_{ca}\kappa_{db} \tag{B12}$$

is the pairing energy. The quantities σ_i correspond to $2s_i$, where s_i is the projection of the intrinsic spin of the state i. We have noted $\widehat{v}^{(a)}_{12} = \widehat{v}_{12}(1 - \widehat{P}_r\widehat{P}_\sigma\widehat{P}_\tau)$ the antisymmetrized interaction. In the following, we consider a central interaction of the type

$$\hat{v}_{12} = (W + B\hat{P}_\sigma - H\hat{P}_\tau - M\hat{P}_\sigma\hat{P}_\tau)G(r)\,F[\rho], \tag{B13}$$

with

$$G(r) = e^{-r^2/p^2}, \quad F[\rho] = \tfrac{1}{2}[\rho^\alpha(\vec{r}_1) + \rho^\alpha(\vec{r}_2)], \tag{B14}$$

and $\vec{r} = \vec{r}_1 - \vec{r}_2$.

The density matrix ρ and the pairing tensor κ appearing in expressions (B10)–(B12) are real and symmetric matrices defined by

$$\rho_{ca} = \langle\widetilde{0}|c^+_a c_c|\widetilde{0}\rangle, \quad \kappa_{ac} = \langle\widetilde{0}|\overline{c_a}c_c|\widetilde{0}\rangle = \sigma_a\langle\widetilde{0}|c_{\overline{a}}c_c|\widetilde{0}\rangle. \tag{B15}$$

The invariance of $|\widetilde{0}\rangle$ by $\widehat{T}$ has for consequences the following relations:

$$\rho_{\overline{ca}} = \sigma_c\sigma_a\,\rho_{ca}, \quad \kappa_{\overline{ac}} = \sigma_a\sigma_c\,\kappa_{ac}. \tag{B16}$$

Moreover, as $|\widetilde{0}\rangle$ is axial, the matrices ρ and κ are diagonals in Ω. They are also diagonal in q in such a way that

$$\begin{aligned} \rho_{ca} &= \delta_{q_a q_c}\delta_{\Omega_a,\Omega_c}\,\rho^{q_a\Omega_a}_{m_c\nu_c,m_a\nu_a}, \\ \kappa_{ca} &= \delta_{q_a q_c}\delta_{\Omega_a,\Omega_c}\,\kappa^{q_a\Omega_a}_{m_c\nu_c,m_a\nu_a}. \end{aligned} \tag{B17}$$

When the parity is imposed, ρ and κ are diagonal according to the parity quantum number π,

$$\rho_{ca} = \delta_{q_a q_c}\delta_{\Omega_a,\Omega_c}\delta_{\pi_a,\pi_c}\,\rho^{q_a\Omega_a\pi_a}_{m_c\nu_c,m_a\nu_a}, \tag{B18}$$

with $\pi_a = (-)^{m_a+n_{za}}$.

The potential $\Gamma^{(\mathrm{tot})}$ is composed by three terms. In the HO representation, its expression is

$$\Gamma^{(\mathrm{tot})}_{ac} = \Gamma_{ac} + \partial\Gamma_{ac} + \partial\Delta_{ac}, \tag{B19}$$

whose definitions of the three terms are given by

$$\Gamma_{ac} = \sum_{bd} \langle ab|\widehat{v}^{(a)}_{12}|cd\rangle \rho_{db}, \tag{B20}$$

$$\partial\Gamma_{ac} = \frac{1}{2} \sum_{bdb'd'} \langle bb'|\frac{\partial\widehat{v}^{(a)}_{12}}{\partial\rho_{ca}}|dd'\rangle \rho_{db}\rho_{d'b'}, \tag{B21}$$

and

$$\partial\Delta_{ac} = \frac{1}{4} \sum_{bdb'd'} \langle b'\overline{d}'|\frac{\partial\widehat{v}^{(a)}_{12}}{\partial\rho_{ca}}|b\overline{d}\rangle \sigma_{d'}\sigma_d\kappa_{d'b'}\kappa_{db}. \tag{B22}$$

The pairing field is

$$\Delta_{ac} = \frac{1}{2} \sum_{bd} \langle a\overline{c}|\widehat{v}^{(a)}_{12}|b\overline{d}\rangle \sigma_c\sigma_d\kappa_{db}. \tag{B23}$$

The interaction being invariant by rotation, parity, and time reversal, the fields Γ, Δ, $\partial\Gamma$, and $\partial\Delta$ have the same diagonal structure (B17) and (B18) as ρ and κ. They obey similar relations as (B16) when the indices a,c are changed to $\overline{a}$,$\overline{c}$.

We note also that, according to the previous relations,

$$V = \frac{1}{2}\sum_{ac}\Gamma_{ac}\rho_{ca}, \quad E_{\mathrm{pair}} = \frac{1}{2}\sum_{ac}\Delta_{ac}\kappa_{ca}. \tag{B24}$$

2. Expression of the field Γ

In the following, we are interested in discussing the field Γ. By making explicit the indices in Eq. (B20) and taking into account the fact that Γ and ρ are diagonal in q and Ω, we obtain

$$\begin{aligned} \Gamma^{q\Omega}_{r_a r_c} = \sum_{q\Omega' r_b r_d} &\langle q s_a m_a \nu_a\, q' s_b m_b \nu_b|\widehat{v}^{(a)}_{12}|q s_c m_c \nu_c\, q' s_d m_d \nu_d\rangle \\ &\times \rho^{q'\Omega'}_{r_d r_b}, \end{aligned} \tag{B25}$$

with $\Omega = m_a + s_a = m_c + s_c$, $\Omega' = m_b + s_b = m_d + s_d$, and $r_a = (m_a,\nu_a)$. Moreover,

$$\widehat{v}^{(a)}_{12} = \widehat{W}_D\; G(r)F[\rho] + \widehat{W}_E\; G(r)F[\rho]\widehat{P}_r, \tag{B26}$$

where

$$\begin{aligned} \widehat{W}_D &= W + B\widehat{P}_\sigma - H\widehat{P}_\tau - M\widehat{P}_\sigma\widehat{P}_\tau, \\ \widehat{W}_E &= M + H\widehat{P}_\sigma - B\widehat{P}_\tau - W\widehat{P}_\sigma\widehat{P}_\tau, \end{aligned} \tag{B27}$$

are the spin-isospin components of direct and exchange fields (in space). We calculate explicitly only the exchange field. The direct field can be deduced by replacing the parameters W,B,H,M with M,H,B,W in the expressions and by omitting $\widehat{P}_r$ in the spatial matrix elements.

Separating the spatial and the spin-isospin parts of the matrix elements of the interaction, the exchange field $\Gamma(E)$ is

$$\Gamma^{q\Omega}_{r_a r_c}(E) = \sum_{q\Omega' r_b r_d} \langle m_a \nu_a \;\; m_b \nu_b | G(r) F[\rho] \widehat{P}_r | m_c \nu_c \;\; m_d \nu_d \rangle \times \langle q s_a \;\; q' s_b | \widehat{W}_E | q s_c \;\; q' s_d \rangle \rho^{q'\Omega'}_{r_d r_b}. \quad \text{(B28)}$$

The spin-isospin matrix element is

$$\begin{aligned} &\langle q s_a \;\; q' s_b | \widehat{W}_E | q s_c \;\; q' s_d \rangle \\ &\quad = \langle s_a s_b | (M - B\delta_{qq'}) + (H - W\delta_{qq'}) \widehat{P}_\sigma | s_c s_d \rangle \\ &\quad = (M - B\delta_{qq'}) \delta_{s_a s_c} \delta_{s_b s_d} + (H - W\delta_{qq'}) \delta_{s_a s_d} \delta_{s_b s_c}. \end{aligned} \quad \text{(B29)}$$

Then

$$\Gamma^{q\Omega}_{r_a r_c}(E) = \sum_{\substack{\Omega' m_b m_d \\ \nu_b \nu_d}} \langle m_a \nu_a \;\; m_b \nu_b | G(r) F[\rho] \widehat{P}_r | m_c \nu_c \;\; m_d \nu_d \rangle \times R^{q s_a s_c \Omega'}_{m_d \nu_d m_b \nu_b}(E), \quad \text{(B30)}$$

with

$$R^{q s_a s_c \Omega'}_{m_d \nu_d m_b \nu_b}(E) = \sum_{q'} \left[(M - B\delta_{qq'}) \delta_{s_a s_c} \delta_{m_b, m_d} + (H - W\delta_{qq'}) \times \delta_{m_b, \Omega' - s_c} \delta_{m_d, \Omega' - s_a} \right] \rho^{q'\,\Omega'}_{m_d \nu_d m_b \nu_b}. \quad \text{(B31)}$$

We assume that $\Omega > 0$. As m_a and m_c are positive or equal to zero, differing at maximum by 1 and as Γ is symmetric, we distinguish two cases: $m_a = m_c = m$ and $m_a = m$, $m_c = m + 1$. We discuss only the first case $m_a = m_c = m$. Thus, we have $s_a = s_c = s$. We note $\Omega = m + s$. The interaction $\widehat{v}_{12}$ commutes with $\widehat{J}_z$ and $\widehat{S}_z$. Consequently, we have $m_b = m_d = m'$ in expression (B30). This leads to

$$\Gamma^{q\Omega = m+s}_{m\nu_a, m\nu_c}(E) = \sum_{\Omega' m' \nu_b \nu_d} \langle m \nu_a \;\; m' \nu_b | G(r) F[\rho] \widehat{P}_r | m \nu_c \;\; m' \nu_d \rangle \times R^{q s s \Omega'}_{m' \nu_d m' \nu_b}(E) \quad \text{(B32)}$$

and

$$R^{q s s \Omega'}_{m' \nu_d m' \nu_b}(E) = \sum_{q'} [M - B\delta_{qq'} + (H - W\delta_{qq'}) \delta_{\Omega', m'+s}] \times \rho^{q'\,\Omega'}_{m' \nu_d m' \nu_b}. \quad \text{(B33)}$$

By limiting the summation to $\Omega' > 0$, we obtains

$$\Gamma^{q\Omega = m+s}_{m\nu_a, m\nu_c}(E) = \sum_{\substack{\Omega' > 0 \\ m' \nu_b \nu_d}} \left[\langle m \nu_a \;\; m' \nu_b | G(r) F[\rho] \widehat{P}_r | m \nu_c \;\; m' \nu_d \rangle R^{q s s \Omega'}_{m' \nu_d m' \nu_b}(E) + \langle m \nu_a \;\; -m' \nu_b | G(r) F[\rho] \widehat{P}_r | m \nu_c \;\; -m' \nu_d \rangle R^{q s s -\Omega'}_{-m' \nu_d - m' \nu_b}(E) \right]. \quad \text{(B34)}$$

According to Eqs. (B33) and (B16),

$$\begin{aligned} R^{q s s -\Omega'}_{-m' \nu_d - m' \nu_b}(E) &= \sum_{q'} [M - B\delta_{qq'} + (H - W\delta_{qq'}) \delta_{-\Omega', -m'+s}] \rho^{q'\,-\Omega'}_{-m' \nu_d - m' \nu_b} \\ &= \sum_{q'} [M - B\delta_{qq'} + (H - W\delta_{qq'}) \delta_{\Omega', m'-s}] \rho^{q'\,\Omega'}_{m' \nu_d m' \nu_b} = R^{q -s -s \Omega'}_{m' \nu_d m' \nu_b}(E). \end{aligned} \quad \text{(B35)}$$

We can replace in Eq. (B34) the summation $\sum_{\Omega' > 0\; m'}$ with $\sum_{m' \geqslant 0} \; \sum_{\Omega' = m' \pm s} \Theta(\Omega')$, where Θ is the Heaviside function:

$$\Theta(\Omega) = \begin{cases} 0 & \text{if } \Omega < 0, \\ 1 & \text{if } \Omega > 0. \end{cases} \quad \text{(B36)}$$

We obtain

$$R^{q s}_{m' \nu_d \nu_b} = \sum_{\Omega' = m' \pm s} \Theta(\Omega') R^{q s s \Omega'}_{m' \nu_d m' \nu_b}(E) = \sum_{q'} \left\{ [M + H - (B + W)\delta_{qq'}] \Theta(m' + s) \rho^{q'\,m'+s}_{m' \nu_d m' \nu_b} + (M - B\delta_{qq'}) \Theta(m' - s) \rho^{q'\,m'-s}_{m' \nu_d m' \nu_b} \right\}. \quad \text{(B37)}$$

By taking into account (B35), we obtain (including $\widehat{P}_r$)

$$\Gamma^{q\Omega = m+s}_{m\nu_a, m\nu_c}(E) = \sum_{m' \geqslant 0 \;\; \nu_b \nu_d} \left[\langle m \nu_a \;\; m' \nu_b | G(r) F[\rho] | m' \nu_d \;\; m \nu_c \rangle R^{q s}_{m' \nu_d \nu_b} + \langle m \nu_a \;\; -m' \nu_b | G(r) F[\rho] | -m' \nu_d \;\; m \nu_c \rangle R^{q\,-s}_{m' \nu_d \nu_b} \right]. \quad \text{(B38)}$$

3. Spatial matrix elements

The spatial matrix elements appearing in Eq. (B38) can be written with the help of the functions (A5):

$$v_{r_a r_b, r_c r_d} = \langle m_a \nu_a \;\; m_b \nu_b | G(r) F[\rho] | m_c \nu_c \;\; m_d \nu_d \rangle = \iint d^3 r_1 d^3 r_2 \;\; \phi^*_{m_a \nu_a}(\vec{r_1})\, \phi^*_{m_b \nu_b}(\vec{r_2}) \phi_{m_c \nu_c}(\vec{r_1})\, \phi_{m_d \nu_d}(\vec{r_2})\, G(|\vec{r_1} - \vec{r_2}|) \times \frac{\rho^\alpha(\vec{r_1}) + \rho^\alpha(\vec{r_2})}{2}. \tag{B39}$$

Starting from the generator functions of the HO functions, it is easy to show a property concerning the product of two HO functions,

$$\phi^*_{m_a \nu_a}(\vec{r})\, \phi_{m_c \nu_c}(\vec{r}) = \sum_{\nu_\mu} T^{\nu_\mu}_{m_a \nu_a, m_c \nu_c} \;\; \phi_{00}(\vec{r}) \;\; \phi_{m_c - m_a, \nu_\mu}(\vec{r}), \tag{B40}$$

where the summation on $\nu_\mu = (n_{\perp\mu}, n_{z\mu})$ is limited by

$$\frac{(|X_a - X_c| - |m_a - m_c|)}{2} \leqslant n_{\perp\mu} \leqslant \frac{(X_a + X_c - |m_a - m_c|)}{2} \quad \text{and} \quad |n_{za} - n_{zc}| \leqslant n_{z\mu} \leqslant n_{za} + n_{zc}, \tag{B41}$$

with

$$X_a = 2n_{\perp a} + |m_a|, \quad X_a = 2n_{\perp c} + |m_c|, \quad m_\mu = m_c - m_a. \tag{B42}$$

It can be shown that the T functions appearing in Eq. (B40) can be decomposed into two parts:

$$T^{\nu_\mu}_{m_a \nu_a, m_c \nu_c} = T^{n_{\perp\mu}}_{m_a n_{\perp a}, m_c n_{\perp c}} \times T^{n_{z\mu}}_{n_{za}, n_{zc}}. \tag{B43}$$

The expressions of the functions $T^{n_{\perp\mu}}_{m_a n_{\perp a}, m_c n_{\perp c}}$ are given by

$$T^{n_{\perp\mu}}_{m_a n_{\perp a}, m_c n_{\perp c}} = [n_{\perp a}!\,(n_{\perp a} + |m_a|)!\;\, n_{\perp c}!\,(n_{\perp c} + |m_c|)! n_{\perp\mu}!(n_{\perp\mu} + |m_c - m_a|)!]^{1/2} \times (-)^{n_{\perp a} + n_{\perp c} + n_{\perp\mu}} \sum_m \left[\left(\frac{X+m}{2}\right)! \left(\frac{X-m}{2}\right)! \left(\frac{X'_a + m + m_a}{2}\right)! \left(\frac{X'_a - m - m_a}{2}\right)! \left(\frac{X'_c + m + m_c}{2}\right)! \times \left(\frac{X'_c - m - m_c}{2}\right)! \right]^{-1}, \tag{B44}$$

with

$$X = \frac{X_a + X_c - X_\mu}{2}, \quad X'_a = \frac{X_a - X_c + X_\mu}{2}, \quad X'_c = \frac{X_c - X_a + X_\mu}{2}. \tag{B45}$$

The quantities X, X'_a, and X'_c are integer. The summation on m is limited by the arguments of the factorials that have to be integer and positive or equal to zero. The index has the same parity as X and its value is between $\mathrm{Max}(-X, -X'_a - m_a, -X'_c - m_c)$ (maximum value) and $\mathrm{Min}(X, X'_a - m_a, X'_c - m_c)$ (minimum value).

The expressions of the functions $T^{n_{z\mu}}_{n_{za}, n_{zc}}$ are given by

$$T^{n_{z\mu}}_{n_{za} n_{zc}} = \frac{(n_{za}!\, n_{zc}!\, n_{z\mu}!)^{1/2}}{\left(\frac{n_{za} + n_{zc} - n_{z\mu}}{2}\right)! \left(\frac{n_{za} - n_{zc} + n_{z\mu}}{2}\right)! \left(\frac{n_{zc} - n_{za} + n_{z\mu}}{2}\right)!}, \tag{B46}$$

with $n_{z\mu}$ having the parity of $n_{za} \pm n_{zc}$.

Using the property (B40), we obtain for the expression (B39)

$$v_{r_a r_b, r_c r_d} = \frac{1}{2} \int d^3 r \;\; \rho^\alpha(\vec{r}) \sum_{\nu_\mu} \left[\phi^*_{m_a \nu_a}(\vec{r}) \;\; \phi_{m_c \nu_c}(\vec{r}) \;\; T^{\nu_\mu}_{m_b \nu_b, m_d \nu_d} G_{m_d - m_b, \nu_\mu}(\vec{r}) + \phi^*_{m_b \nu_b}(\vec{r}) \;\; \phi_{m_d \nu_d}(\vec{r}) T^{\nu_\mu}_{m_a \nu_a, m_c \nu_c} G_{m_c - m_a, \nu_\mu}(\vec{r}) \right], \tag{B47}$$

with

$$G_{m_\mu \nu_\mu}(\vec{r}) = \int d^3 r' \;\; G(|\vec{r} - \vec{r'}|) \;\; \phi_{00}(\vec{r'}) \;\; \phi_{m_\mu \nu_\mu}(\vec{r'}). \tag{B48}$$

The quantity $G_{m_\mu \nu_\mu}(\vec{r})$ can be calculated analytically. Its expression is

$$G_{m_\mu \nu_\mu}(\vec{r}) = \frac{(\pi p^2)^{3/2}}{G_\perp^{\frac{2n_{\perp\mu} + |m_\mu| + 2}{2}} G_z^{\frac{n_{z\mu} + 1}{2}}} \;\; \phi_{000}\left(\frac{\vec{r}_\perp}{\sqrt{G_\perp}}, \frac{z}{\sqrt{G_z}}\right) \phi_{m_\mu n_{\perp\mu} n_{z\mu}}\left(\frac{\vec{r}_\perp}{\sqrt{G_\perp}}, \frac{z}{\sqrt{G_z}}\right), \tag{B49}$$

with

$$G_\perp = 1 + \beta_\perp p^2, \quad G_z = 1 + \beta_z p^2, \tag{B50}$$

where β_z and $\beta_\perp$ are the parameters of the HO along the z axis and $\vec{r}_\perp$. One sees that $G_{m_\mu \nu_\mu}$ depends on the angle φ contained in $\vec{r}_\perp$ only through the phase $e^{i m_\mu \varphi}$ of $\phi_{m_\mu n_{\perp\mu} n_{z\mu}}$. Then we can write

$$G_{m_\mu \nu_\mu}(\vec{r}) = e^{i m_\mu \varphi} G_{|m_\mu| \nu_\mu}(\widetilde{r}), \tag{B51}$$

with

$$G_{|m_\mu| \nu_\mu}(\widetilde{r}) = \frac{(\pi p^2)^{3/2}}{G_\perp^{\frac{2n_{\perp\mu}+|m_\mu|+2}{2}} G_z^{\frac{n_{z\mu}+1}{2}}} \phi_{000}\left(\frac{r_\perp}{\sqrt{G_\perp}}, \frac{z}{\sqrt{G_z}}\right) \phi_{|m_\mu| n_{\perp\mu} n_{z\mu}}\left(\frac{r_\perp}{\sqrt{G_\perp}}, \frac{z}{\sqrt{G_z}}\right). \tag{B52}$$

We have denoted $\phi_{|m|\nu}(\widetilde{r})$ as the HO wave function left without its phase $e^{im\varphi}$ and $\widetilde{r} = (r_\perp, z)$. Substituting Eq. (B51) in Eq. (B47), we see that the integration on the angle φ implies $m_a + m_b = m_c + m_d$ because the density $\rho(\vec{r})$ is axial and depends only on $\widetilde{r}$. This equality was expected as the interaction $G(r)F[\rho]$ in (B39) preserves $\widehat{J}_z$. Hence,

$$v_{r_a r_b, r_c r_d} = \pi \int d^2\widetilde{r}\, \rho^\alpha(\widetilde{r}) \sum_{\nu_\mu} \left[T^{\nu_\mu}_{m_a \nu_a, m_c \nu_c} \phi_{|m_b|\nu_b}(\widetilde{r})\, \phi_{|m_d|\nu_d}(\widetilde{r}) + T^{\nu_\mu}_{m_b \nu_b, m_d \nu_d} \phi_{|m_a|\nu_a}(\widetilde{r})\, \phi_{|m_c|\nu_c}(\widetilde{r})\right] G_{|m_c - m_a|\nu_\mu}(\widetilde{r}). \tag{B53}$$

It is convenient to define

$$\widetilde{G}_{m_a \nu_a, m_c \nu_c}(\widetilde{r}) = \sum_{\nu_\mu} T^{\nu_\mu}_{m_a \nu_a, m_c \nu_c} G_{|m_c - m_a|\nu_\mu}(\widetilde{r}). \tag{B54}$$

The quantity (B54) is symmetric in $m_a \nu_a$ and $m_c \nu_c$ and it is invariant in the simultaneous exchange m_a in $-m_a$ and m_c in $-m_c$,

$$\widetilde{G}_{m_a \nu_a, m_c \nu_c}(\widetilde{r}) = \widetilde{G}_{m_c \nu_c, m_a \nu_a}(\widetilde{r}) = \widetilde{G}_{-m_a \nu_a, -m_c \nu_c}(\widetilde{r}), \tag{B55}$$

because the coefficient T has the same properties.

Finally, we obtain

$$\langle m_a \nu_a \;\; m_b \nu_b | G(r) F[\rho] | m_c \nu_c \;\; m_d \nu_d \rangle = \pi \int d^2\widetilde{r}\, \rho^\alpha(\widetilde{r}) \left[\phi_{|m_a|\nu_a}(\widetilde{r}) \phi_{|m_c|\nu_c}(\widetilde{r}) \widetilde{G}_{m_b \nu_b, m_d \nu_d}(\widetilde{r}) + \phi_{|m_b|\nu_b}(\widetilde{r}) \phi_{|m_d|\nu_d}(\widetilde{r}) \widetilde{G}_{m_a \nu_a, m_c \nu_c}(\widetilde{r})\right]. \tag{B56}$$

The field (B38) has for expression

$$\begin{aligned} \Gamma^{q\Omega=m+s}_{m\nu_a, m\nu_c}(E) = \pi \int d^2\widetilde{r}\, \rho^\alpha(\widetilde{r}) \sum_{m' \geqslant 0 \nu_b \nu_d} \phi_{|m'|\nu_d}(\widetilde{r}) \Big\{ &\left[\phi_{|m|\nu_a}(\widetilde{r}) \widetilde{G}_{m\nu_c, m'\nu_b}(\widetilde{r}) + \phi_{|m|\nu_c}(\widetilde{r}) \widetilde{G}_{m\nu_a, m'\nu_b}(\widetilde{r})\right] R^{qs(+)}_{m'\nu_d \nu_b} \\ &+ \left[\phi_{|m|\nu_a}(\widetilde{r}) \widetilde{G}_{m\nu_c, -m'\nu_b}(\widetilde{r}) + \phi_{|m|\nu_c}(\widetilde{r}) \widetilde{G}_{m\nu_a, -m'\nu_b}(\widetilde{r})\right] R^{qs(-)}_{m'\nu_d \nu_b} \Big\}, \end{aligned} \tag{B57}$$

with

$$R^{qs(\pm)}_{m'\nu_d \nu_b} = \sum_{q'} \left\{[M + H - (B + W)\delta_{qq'}]\Theta(m' \pm s) \rho^{q' m' \pm s}_{m'\nu_d, m'\nu_b} + (M - B\delta_{qq'})\Theta(m' \mp s) \rho^{q' m' \mp s}_{m'\nu_d, m'\nu_b}\right\}. \tag{B58}$$

The expressions with $F[\rho] = 1$ are obtained by taking $\alpha = 0$. Moreover, if we replace $G(r)$ with $\delta(\vec{r})$, we recover the expression of the zero-range density term of the standard Gogny interaction.

[1] T. H. R. Skyrme, Philos. Mag. **1**, 1043 (1956).
[2] T. H. R. Skyrme, Nucl. Phys. **9**, 615 (1958).
[3] N. V. Giai, D. Vautherin, M. Vénéroni, and D. M. Brink, Phys. Lett. B **35**, 135 (1971).
[4] D. Vautherin, Ph.D. thesis, Université de Paris, 1969.
[5] D. Vautherin, M. Vénéroni, and D. M. Brink, Phys. Lett. B **33**, 381 (1970).
[6] D. Vautherin and D. M. Brink, Phys. Lett. B **32**, 149 (1970).
[7] D. Vautherin and D. M. Brink, Phys. Rev. C **5**, 626 (1972).
[8] D. Vautherin and D. M. Brink, Phys. Rev. C **7**, 296 (1973).
[9] E. Chabanat, P. Bonche, P. Haensel, J. Meyer, and R. Schaeffer, Nucl. Phys. A **627**, 710 (1997).
[10] E. Chabanat, P. Bonche, P. Haensel, J. Meyer, and R. Schaeffer, Nucl. Phys. A **635**, 231 (1998).
[11] G. Colò, H. Sagawa, S. Fracasso, and P.-F. Bortignon, Phys. Lett. B **646**, 227 (2007).
[12] T. Lesinski, M. Bender, K. Bennaceur, T. Duguet, and J. Meyer, Phys. Rev. C **76**, 014312 (2007).
[13] M. Kortelainen, T. Lesinski, J. Moré, W. Nazarewicz, J. Sarich, N. Schunck, M. V. Stoitsov, and S. Wild, Phys. Rev. C **82**, 024313 (2010).

[14] M. Dutra, O. Lourenco, J. S. Sa Martins, A. Delfino, J. R. Stone, and P. D. Stevenson, Phys. Rev. C **85**, 035201 (2012). See for example Table II.

[15] D. Gogny, in *Proceeding of the International Conference on Nuclear Physics, Munich*, edited by J. De Boer and H. J. Mang, (North-Holland, Amsterdam, 1973), Vol. 1, p. 48.

[16] D. Gogny, in *Nuclear Self-Consistent Fields, Trieste*, edited by G. Ripka and M. Porneuf (North-Holland, Amsterdam, 1975), p. 333.

[17] J. Dechargé and D. Gogny, Phys. Rev. C **21**, 1568 (1980).

[18] J.-F. Berger, M. Girod, and D. Gogny, Nucl. Phys. A **502**, 85 (1989).

[19] J.-F. Berger, M. Girod, and D. Gogny, Comput. Phys. Commun. **63**, 365 (1991).

[20] G. A. Lalazissis, J. König, and P. Ring, Phys. Rev. C **55**, 540 (1997).

[21] T. Niksic, D. Vretenar, P. Finelli, and P. Ring, Phys. Rev. C **66**, 024306 (2002).

[22] G. A. Lalazissis, T. Niksic, D. Vretenar, and P. Ring, Phys. Rev. C **71**, 024312 (2005).

[23] S. Kohler, Nucl. Phys. A **258**, 301 (1976).

[24] S. Shlomo, V. M. Kolomietz, and G. Colò, Eur. Phys. J. A **30**, 23 (2006).

[25] H. Nakada, Phys. Rev. C **68**, 014316 (2003).

[26] H. Nakada, Phys. Rev. C **87**, 014336 (2013).

[27] J.-P. Blaizot and D. Gogny, Nucl. Phys. A **284**, 429 (1977).

[28] D. Gogny and R. Padjen, Nucl. Phys. A **293**, 365 (1977).

[29] J. P. Blaizot, J. F. Berger, J. Dechargé, and M. Girod, Nucl. Phys. A **591**, 435 (1995).

[30] S. Péru, J. F. Berger, and P. F. Bortignon, Eur. Phys. J. A **26**, 25 (2005).

[31] V. De Donno, G. Co, C. Maieron, M. Anguiano, A. M. Lallena, and M. Moreno Torres, Phys. Rev. C **79**, 044311 (2009).

[32] V. De Donno, G. Co, M. Anguiano, and A. M. Lallena, Phys. Rev. C **83**, 044324 (2011).

[33] S. Péru and H. Goutte, Phys. Rev. C **77**, 044313 (2008).

[34] S. Péru, G. Gosselin, M. Martini, M. Dupuis, S. Hilaire, and J.-C. Devaux, Phys. Rev. C **83**, 014314 (2011).

[35] J.-P. Delaroche, M. Girod, J. Libert, H. Goutte, S. Hilaire, S. Péru, N. Pillet, and G. F. Bertsch, Phys. Rev. C **81**, 014303 (2010).

[36] L. M. Robledo and G. F. Bertsch, Phys. Rev. C **84**, 054302 (2011).

[37] R. Rodriguez-Guzman, P. Sarriguren, and L. M. Robledo, Phys. Rev. C **82**, 044318 (2010).

[38] D. Gambacurta, F. Catara, and M. Grasso, Phys. Rev. C **80**, 014303 (2009)

[39] D. Gambacurta, M. Grasso, and F. Catara, Phys. Rev. C **84**, 034301 (2011).

[40] D. Gambacurta, M. Grasso, V. De Donno, G. Co, and F. Catara, Phys. Rev. C **86**, 021304 (2012).

[41] N. Pillet, J.-F. Berger, and E. Caurier, Phys. Rev. C **78**, 024305 (2008).

[42] N. Pillet, V. G. Zelevinsky, M. Dupuis, J.-F. Berger, and J.-M. Daugas, Phys. Rev. C **85**, 044315 (2012).

[43] J. Le Bloas, N. Pillet, M. Dupuis, J.-M. Daugas, L. Robledo, C. Robin, and V. G. Zelevinsky, Phys. Rev. C **89**, 011306(R) (2014).

[44] F. Raimondi, B. G. Carlsson, and J. Dobaczewski, Phys. Rev. C **83**, 054311 (2011).

[45] J. Sadoudi, T. Duguet, J. Meyer, and M. Bender, Phys. Rev. C **88**, 064326 (2013).

[46] F. Chappert, Ph.D. thesis, Université Paris-Sud XI, Number 8672, 2007, http://www.theses.fr/2007PA112134

[47] L. M. Robledo, R. N. Bernard, and G. F. Bertsch, Phys. Rev. C **89**, 021303 (2014).

[48] F. Chappert, M. Girod, and S. Hilaire, Phys. Lett. B **668**, 420 (2008).

[49] S. Goriely, S. Hilaire, M. Girod, and S. Péru, Phys. Rev. Lett. **102**, 242501 (2009).

[50] M. Anguiano, G. Co, V. De Donno, and A. M. Lallena, Phys. Rev. C **83**, 064306 (2011).

[51] http://www-phynu.cea.fr/

[52] B. H. Brandow, Master's thesis, Cornell University, 1964.

[53] B. Frois and C. Papanicolas, Annu. Rev. Nucl. Part. Sci. **37**, 133 (1987).

[54] W. D. Myers and W. J. Swiatecki, Nucl. Phys. **81**, 1 (1966).

[55] W. D. Myers, Nucl. Phys. A **145**, 387 (1970).

[56] W. D. Myers and W. J. Swiatecki, Ann. Phys. (NY) **55**, 395 (1969).

[57] P. Möller and J. R. Nix, Nucl. Phys. A **520**, c369 (1990).

[58] P. Möller, J. R. Nix, W. D. Myers, and W. J. Swiatecki, At. Data Nucl. Data Tables **59**, 185 (1995).

[59] C. Mahaux and R. Sartor, Adv. Nucl. Phys. **20**, 1 (1991).

[60] M. Baldo and A. Eldeen Shaban, Phys. Lett. B **661**, 373 (2008).

[61] M. Baldo (private communication).

[62] R. B. Wiringa, R. A. Smith, and T. L. Ainsworth, Phys. Rev. C **29**, 1207 (1984); R. B. Wiringa, V. G. J. Stoks, and R. Schiavilla, *ibid.* **51**, 38 (1995).

[63] B. Friedman and V. R. Pandharipande, Nucl. Phys. A **361**, 502 (1981).

[64] E. N. E. van Dalen, C. Fuchs, and A. Faessler, Phys. Rev. Lett. **95**, 022302 (2005).

[65] I. Bombaci and U. Lombardo, Phys. Rev. C **44**, 1892 (1991).

[66] B.-A. Li, Phys. Rev. C **69**, 064602 (2004).

[67] L. D. Landau, JETP (Sov. Phys.) **32**, 59 (1957).

[68] M. Bender, J. Dobaczewski, J. Engel, and W. Nazarewicz, Phys. Rev. C **65**, 054322 (2002).

[69] J. Margueron, J. Navarro, N. Van Giai, and P. Schuck, Phys. Rev. C **77**, 064306 (2008).

[70] D. Davesne, A. Pastore, and J. Navarro, Phys. Rev. C **89**, 044302 (2014).

[71] A. Pastore, D. Davesne, K. Bennaceur, J. Meyer, and V. Hellemans, Phys. Scr. T **1154**, 014014 (2013).

[72] S. O. Bäckman, A. D. Jackson, and J. Speth, Phys. Lett. B **56**, 209 (1975).

[73] S. O. Bäckman, G. E. Brown, and J. A. Niskanen, Phys. Rep. **124**, 1 (1985).

[74] J. Speth, L. Zamick, and P. Ring, Nucl. Phys. A **232**, 1 (1974).

[75] P. Ring and J. Speth, Phys. Lett. B **44**, 477 (1973).

[76] P. Ring and J. Speth, Nucl. Phys. A **235**, 315 (1974).

[77] A. B. Migdal, *Theory of Finite Fermi Systems and Applications to Atomic Nuclei* (Interscience, New York, 1967).

[78] V. Baran, M. Colonna, M. Di Toro, and V. Greco, Phys. Rev. Lett. **86**, 4492 (2001).

[79] J. Margueron and Ph. Chomaz, Phys. Rev. C **67**, 041602(R) (2003).

[80] J. Margueron, J. Navarro, and P. Blottiau, Phys. Rev. C **70**, 028801 (2004).

[81] E. Garrido, P. Sarriguren, E. Moya de Guerra, and P. Schuck, Phys. Rev. C **60**, 064312 (1999).

[82] http://www.nndc.bnl.gov/ensdf/
[83] T. T. S. Kuo, E. U. Baranger, and M. Baranger, Nucl. Phys. **79**, 513 (1966).
[84] N. Pillet, N. Sandulescu, and P. Schuck, Phys. Rev. C **76**, 024310 (2007).
[85] N. Pillet, N. Sandulescu, P. Schuck, and J.-F. Berger, Phys. Rev. C **81**, 034307 (2010).
[86] W. Heisenberg, Z. Phys. **78**, 156 (1932).
[87] A. Bohr and B. R. Mottelson, *Nuclear Structure*, 1st ed. (World Scientific, Singapore, 1998).
[88] W. Satula, J. Dobaczewski, and W. Nazarewicz, Phys. Rev. Lett. **81**, 3599 (1998).
[89] T. Duguet, P. Bonche, P.-H. Heenen, and J. Meyer, Phys. Rev. C **65**, 014311 (2001).
[90] P. Ring and P. Schuck, *The Nuclear Many-body Problem* (Springer-Verlag, New York, 1980).
[91] G. Audi and A. H. Wapstra, Nucl. Phys. A **595**, 409 (1995).
[92] E. N. M. Quint *et al.*, Phys. Rev. Lett. **58**, 1088 (1987).
[93] M. Dupuis, S. Karataglidis, E. Bauge, J. P. Delaroche, and D. Gogny, Phys. Rev. C **73**, 014605 (2006).
[94] E. W. Otten, in *Treatise on Heavy-Ion Science*, edited by D. A. Bromley (Plenum, New York, 1989), Vol. 7, p. 517.
[95] I. Angeli, At. Data Nucl. Data Tables **87**, 185 (2004).
[96] M. M. Sharma, G. A. Lalazissis, and P. Ring, Phys. Lett. B **317**, 9 (1993).
[97] P. G. Reinhard and H. Flocard, Nucl. Phys. A **584**, 467 (1995).
[98] S. Raman, C. W. Nestor, and P. Tikkanen, At. Data Nucl. Data Tables **78**, 1 (2001).
[99] D. R. Inglis, Phys. Rev. **103**, 1786 (1956).
[100] S. T. Belyaev, Nucl. Phys. **24**, 322 (1961).
[101] J. Libert, M. Girod, and J.-P. Delaroche, Phys. Rev. C **60**, 054301 (1999).
[102] D. J. Thouless and J. G. Valatin, Nucl. Phys. **31**, 211 (1962).
[103] Reference Input Parameter Library-2, IAEA, Vienna (2002), tecDoc (2003), unpublished, www-nds.iaea.org/ripl/
[104] G. N. Smirenkin, Report INDC (CCP)-359, 1993, unpublished, www-nds.iaea.org/ripl/